**Department of Imaging and Applied Physics**
**Centre for Marine Science and Technology**

# Tidal Modeling in Correlation to Prevailing Meteorological Conditions in Torres Strait, Australia

**Nina Ribbat**

**This thesis is presented in Partial Fulfillment of the Requirements for the Degree of Master of Science by Coursework**

**of**

**Curtin University of Technology**

**May 2012**

This project is part of the Masters of Science by Coursework in Applied Physics conducted by the Department of Applied Physics, Curtin University of Technology.

# Abstract

This thesis describes the application of a multiple regression technique to forecast tidal residuals due to meteorological conditions in Torres Strait, Australia. 3 years of tidal data at 5 tide gauge stations in the vicinity of the Prince of Wales Channel, Torres Srait, Australia, were obtained from the Australian Maritime Safety Authority (AMSA). Tidal harmonic constituents were determined from the observed tidal signal and used to reconstruct the residual time series. In this study, only westerly winds and atmospheric pressure were considered. Examination of the residuals indicated that Booby Island has the strongest response to meteorological conditions, whereas Nardana Patches and Ince Point, located towards the eastern part of the channel, show a weak response. A linear scheme has been established incorporating a combination of time lags of previous meteorological data. The long-term prediction of residual tides has been found to be underestimated. It is suggested that oscillations in the shipping channel may have their origin the Arafura Sea-Gulf system.

# Table of Contents

# List of Tables

# List of Figures

# Chapter 1. Introduction and Background

*Perhaps no space of 3 ½ ° in length, presents more dangers than Torres Strait, but with caution and perseverance the Captains Bligh and Portlock proved them to be surmountable*

Matthew Flinders, 1803

## 1.1 Introduction

Gravitational tidal forces are known to be the largest source of short-term sea-level fluctuations throughout our ocean basins (Godin 1972). However, the sources, dynamics and consequences of these forces in shallow seas have not been well understood. Of particular complexity are nearshore environments, where sea levels not only fluctuate under the synergetic influence of changing tides, but also under meteorological forcing. The knowledge of non-tidal sea level fluctuations in these environments is of great importance for the navigation of vessels as well as for planning coastal communities and monitoring marine ecosystems. Numerical models provide a useful tool to enhance the understanding of basic ocean processes but the complex geometry and shallow nature of the coastal ocean coupled with linear and non-linear effects makes numerical modelling extremely sensitive to errors. This study examines non - tidal sea level oscillations due to atmospheric conditions in the shallow waters of Torres Strait, Australia.

In providing direct access from Northern Australia and Southeast Asia to the east coast of Australia, New Zealand and South Pacific, Torres Strait plays a significant

role for the national and international economy (Forbes et al. 1983). The search for mechanisms responsible for the generation of non-tidal sea level fluctuations in Torres Strait is also of considerable interest to native communities who mainly depend on natural resources for commercial and traditional purposes, as well as to local fisheries operating in the area (Bode et al. 1994). The Torres Strait has therefore been recognized as the most important environment to the economic development of the local and surrounding regions.

General driving forces of the circulation in Torres Strait have been well documented in the literature. However, less attention has been paid to quantifying the dominant meteorological forcing mechanisms governing sea level fluctuations within the main shipping channels. The necessity for improved tidal predictions in Torres Strait becomes evident by reviewing the number of recorded ship incidents. A study conducted by AMSA found that 40 major incidents occurred in a time period of 15 years between 1985 and 2000 in the Great Barrier Reef and Torres Strait region consisting of 26 groundings and 14 collisions. The increasing value of natural Australian resources within the Asian Pacific region will increase the demand for shipping services to the Torres Strait and the Great Barrier Reef region by an estimated value of 36 per cent between 2010 and 2020 (ABS 2001).

Shallow and reef covered areas impose great difficulties upon the navigating pilot to avoid a grounding or collision. Ship groundings have a substantial impact not only on the localized seafloor, but also on the existing reef structure. Increased water turbidity caused by the sudden impact will diminish light penetration through the water column alternating the reefs natural environment (Schroeder et al. 2008). Since observations to date clearly indicate the potential for future groundings in this economically and environmentally sensitive area, knowledge of local sea level fluctuations is crucial to reduce and prevent incidents.

Sea level fluctuations are the response to numerous stimuli. As stated earlier, periodic oscillations resulting from the gravitational interaction and motion of the Sun, Moon and Earth acting on ocean waters have been known as gravitational tides for

centuries. Since the orbital paths of these bodies are to date exactly known, relative changing positions and corresponding gravitational forces between the bodies are used as a basis to establish predictions for tide heights and times throughout the world (Godin 1972). But tidal regimes differ throughout locations with varying tidal heights and times. These tidal changes are the overall result of multiple influences that act over varying periods known as tidal constituents. The primary constituents are the earth's rotation; the positions of Moon and the Sun relative to Earth, the moon's altitude above the earth, and bathymetry. Each constituent symbolizes a variation in the relative positions of the Earth, Moon and Sun.

Other stimuli impacting sea level elevation, particularly in shallow areas such as Torres Strait, are spatial variations in barometric pressure and the operation of wind stress on the sea surface. At times, these conditions interact in a complex way to elevate or lower water levels significantly above or under predicted tide heights. Surges generated through these meteorological conditions induce great navigational hazards. Furthermore, periods of strong winds blowing straight onshore over the ocean’s surface cause water pile up against coast lines and reefs systems, while winds blowing offshore reverses the effect with causing the water level to be depressed in height (Godin 1972). The degree of pile up depends on the topography of the area. Some of the pile up water may returns as bed flow; however, in extensive shallow reef areas the shear between the bed return flow and the surface water may limit return flow. Shallow reef areas will therefore experience a greater water pile up due to restricted passageways for the incoming water. Pressure systems may rise or lower the sea level height dependent on the type of the prevailing system. Low pressure systems elevate sea levels, whereas high pressure systems tend to depress it as a result of the inverted barometric effect. However, the water level height adjusts itself slowly to the average change of barometric pressure over a considerable area (Wolanski 1988). The effect of pressure induced oscillations in water sea level elevation is therefore considerably small. But the combination of wind induced water pile up and the inverted barometer effect associated with storms can generate a dangerous increase in sea level elevation. Unusually low water levels are associated with high pressure systems and offshore winds. Those

changes in water elevation are of great importance to vessels navigating through shallow shipping channels with small under-keel clearances. It follows that the prediction of water level heights in shallow regions therefore requires both the inclusion of meteorological and astronomical forcing functions.

Local sea level elevation is generally determined using tidal harmonic analysis, a mathematical method to represent and hint cast future tide times/heights. It can further be described as an extrapolative process based on a series of observations at a specific place (Hemer 2003). General tidal predictions are based on average seasonal meteorological conditions, neglecting the impact of local weather and oceanographic effects on sea level heights. But major variations in those conditions will cause corresponding differences between the predicted and actual tide height (Csanady 1973) known as residuals. The concept of residuals arises from the occurrence of tidal anomalies due to non-planetary effects such as wind and barometric setup, ocean swell and local wind waves. But also the configuration of the coastline and its associated bathymetry may also have an effect on the tidal regime. Another considerable factor in tidal patterns is the anthropogenic influence which can also have the ability to change the local tidal regime by modifying the local and adjacent topography (Csanady 1973). A residual tidal component is generally speaking a quantity left over at the end of the comparison process of actual and predicted tidal heights, indicating the performance level of tidal predictions. In this study, observations of large tidal residual peaks led to a working hypothesis that non-tidal oscillations are driven by atmospheric conditions. As a result, the overall objective of this study is to investigate the hypothesis that periods of strong west winds in Torres Strait distort the predicted tidal signal. The approach is to formulate a technique using regression analysis which allows the direct inclusion of prevailing meteorological conditions to forecast discrepancies in tidal predictions. Investigating this issue is vital in lessen navigational hazards in the shipping channels of Torres Strait region.

In addition, the research proposed here will expand our efforts to improve knowledge of nearshore sea level fluctuations in the shallow reef enclosed areas of the Great Barrier Reef and Torres Strait region. It will also promote on-going research,

which is currently conducted in Torres Strait by the Australian Reef Pilots regarding the improvement of navigation systems through shallow parts of the Strait.

### 1.1.1 Introduction to Tidal Analysis and Prediction Techniques

Over the centuries knowledge of global oceanic tides has immensely advanced and various theories have since been proposed to explain and predict oceanic tides. Technological inventions such as oceanic pressure gauges and satellite altimeters have further enhanced the understanding of global and local tidal dynamics. General open ocean tides have been well modeled and predicted by scientist around the world using various ocean tide models. Tides in shallow waters on the other hand, have been far less documented in the literature. The complex and shallow bathymetry coupled with strong mixed tidal patterns in Torres Strait induce great difficulties for local tidal predictions. In this section, previous methods of tidal predictions used in shelf and near –coastal regions are reviewed. Furthermore, current approaches in modeling tides in Torres Strait are presented including descriptions of methods used (Knight 1981).

The dynamic analysis of oceanic time series recorded by pressure gauges is fundamental in regards to the understanding and prediction of local tidal dynamics. Since the days of George Darwin, tide recordings have been investigated for amplitude and phase information at periods associated with the orbital motion of the sun and the moon. It was believed that tide records could be reproduced to a desired accuracy depending on the number of periods included. Tidal signals, however, do not exist by themselves; they rather contain a complex combination of the periodic oscillations caused by the gravitational forces of the moon and the sun acting on the ocean and irregular oscillations due to atmospheric and oceanic variability. Thus, as described by Munk and Cartwright (1966), the pure astronomical tidal response is a superposition on an overall noisy spectrum, the so called continuum. Pawlowicz (2002) shows the separation of tidal from non – tidal energy is a crucial component in any analysis of oceanic time series, especially in shelf and near coastal waters.

Gravitational forces exerted from the sun and the moon varies spatially due to the rotation of the earth around its axis. Thus, oceanic responses in deep open waters are mainly the result of astronomical forces whereas tidal effects in near coastal regions occur as a combination of waves propagating through shallower coastal waters as a residue of deep oceanic variability. Power spectra of typical oceanic time series show high energies in the low frequency range with declining energy peaks at higher frequencies. Furthermore, the power spectrum reveals the superimposition of various sharp peaks associated with astronomical periods near diurnal and semidiurnal frequencies. Inertial and coriolis effects arise as broader peaks throughout the spectra. It follows that a dynamic analysis of oceanic time series requires the separation of the tidal signal from existing tidal variations. In shallow regions inertial effects at closely related frequencies must be as well separated from the astronomical signal. Various methods have been developed to achieve the separation of the tidal response from oceanic time series. The application of low and high band pass filtering techniques has been found to be rather inefficient as a consequence of the deterministic nature and large amplitudes of the tidal signal requiring narrow filters with a high amount of rejection. Nevertheless, they present a useful tool in the analysis of the residual time series (non-astronomical components of the signal).

The classic method of determining the amplitudes and phases of the tidal response by applying the Fast Fourier transform is of limited success for the following reasons. The frequencies computed by the definition of the discrete Fourier transform normally do not coincide with the frequencies of the existing tidal harmonics, especially if the length of the transform, N, is chosen to perform well with a Fast Fourier transform algorithm. Further problems with fast Fourier analysis arise from the fact that the noise level is assumed to be equal at all frequencies, even though noise levels have been observed to be unsteady throughout the signal with increased noise levels in the tidal bands. This phenomenon is known as tidal cusping (Munk et al., 1965; Ponchaut et al., 2001; Colosi and Munk, 2006).

The cross-spectral technique described by Munk and Cartwright in 1966 has the advantage of providing estimates of the noise as a function of frequency taking varying noise levels into account. The core of this method is to find the cross-spectrum between

a noise-free reference series and the time series. This is achieved by using a slow Fourier transform to modify the Fourier frequencies so they are closer to the tidal frequencies. The next step is to reduce bias noise from spectral leakage by windowing the time series and averaging to obtain a statistically consistent estimate. However, for this method to produce reliable results, long data sets are required, which might not also be the case, depending on the desired tide records. The full procedure is described in detail by Munk and Cartwright (1966).

The most widely used technique for tidal analysis is the classic harmonic method, first introduced by Lord Kelvin and Sir George Darwin in 1867. The tidal signal is synthesized as the sum of a finite set of sinusoids at predetermined frequencies due to gravitational forcing mechanisms of planetary motions. These particular frequencies are a combination of the Doodsen numbers which represent the set of 6 signed integers needed to represent a particular frequency caused by gravitational interactions of terrestrial and celestial bodies. The least squares harmonic analysis method (Hamels method) has a variety of advantages (Emery and Thomspon 2001. As there are hundreds of tidal frequencies, many so closely related in frequency that large data sets are required to be adequately resolved. The least squares fit permit the resolution of a large number of constituents given a long enough data set Since there are only 45 astronomical constituents, the remaining constituents are classified as compound and over tides which arise from bottom frictional and atmospheric effects as well as from non-linear terms in the equations of motion. With increasing length of the data set further constituents can be added to the analysis. The primary aim of the least squares analysis is to produce estimates of the phases and amplitudes of the particular tidal harmonic constituents by minimizing the sum of squares of residuals. The fitting of m sine-cosine pairs with specified frequencies $f_l$ to the number of data points $N$ from the time series $y_n$ can be expressed as follows by minimizing the function

$$\sum_{n=0}^{N}\left[y_n - \sum_{l=1}^{m}\left(A_l \cos\left(2\pi f_l t_n\right) + B_l \sin\left(2\pi f_l t_n\right)\right)\right]^2$$

where the specific frequencies $f$ represent the predetermined tidal harmonic frequencies and the A's and B's represent the unknown amplitudes being solved for

(Magori 2008). The obtained phases and amplitudes can then be further used for prediction purposes.

A major drawback to the least squares analysis, as described by Agnew in 1964, is the fact that it is assumed that the residuals after fitting the sinusoids will be consisting of independent random variables. However, this particular case is only valid if the existing noise spectrum consists of white noise only. The continuum of most tide records contains more white noise as well as long-period noises outside the known tidal bands. Thus, the signal can be run through a filter before the actual analysis (Agnew 2007). Another major drawback of the least squares method is the earlier mentioned effect of tidal cusping, where the noise level dramatically increases within the tidal bands. It follows that for the method of least squares to give reliable results; error bands must be accounted for in the analysis otherwise error bands might be over or underestimated for amplitudes and phases.

Another weakness of classical harmonic analysis arises from the previous observation: If the amplitude and phase information found via the least squares fit is truly a tidal signal, or if the resulting result is due to excess energy within the tidal bands. Also, the question whether the resulting amplitude and phases stem from fitting to a component of the continuum (the non-tidal spectrum) or the real tidal signal has to be addressed (Pawlowicz et al 2002). Further errors may arise from neglecting the nodal modulations, in particular the modulation of the perihelion, which requires a time series of about 18.6 years of length to adequately resolve all constituents (Pawlowicz et al 2002). Since most time series are much shorter in length and rarely exceed a length of one year, this instability is continuous and occurs when fitting to amplitudes of harmonics separated in frequency by less than 1/N, where N is the length of the time series (Agnew, Munk and Hasselmann 1964). This issue is not limited to nodal modulations in particular, depending on the length of the time series, certain tidal harmonic frequencies cannot be resolved properly since they are separated by only 0.15 cycles /month. To address this issue, closely related tidal harmonic frequencies are taken as reference points with the assumption that the ocean response should be similar at those frequencies. Thus, the frequency bands are a combination of large equilibrium

and small peaks, which represent nodal modulations. It follows that the resulting tidal harmonic sinusoids appear as slowly varying functions. In shelf and near coastal regions another complexity is added to the analysis due to the interaction of the local topography with the changing phases of the tides. The above mentioned drawbacks to tidal harmonic analysis add further complexity to the analysis of tidal records.

As mentioned before, the length of a tidal signal plays a key role in resolving particular tidal harmonic frequencies. Since there are many tidal frequencies with minimal separation between them, long data sets are a necessity to effectively resolve them. Computation cost and time of computer programs increases with an increasing number of constituents which also encourages the sensitive choice of constituents. Since most tidal records span a time record of less than a year, it is not reasonable to include all constituents. Godin (1972) describes the Rayleigh separation criterion to narrow the choice of constituents allowed in the analysis. The inclusion of two main constituents is mainly dependent on the record length and the choice of the Rayleigh constant, which is in general set to be 1. Two chosen constituents are permitted in the analysis if the number of cycles between the two frequencies over the period T exceeds the value of Ray. That is

$$\left| f_2 - f_1 \right| t > Ray$$

where $f_1$, $f_2$ are main tidal harmonic constituents, t is the record length and Ray is the Rayleigh constant. In case this criterion has not been met, further decisive factors have to be introduced in order to decide which constituent to add in the inclusion. Forman (1977) introduced Rayleigh comparison pairs, based on tidal potential amplitude, as a reference point in the inclusion of tidal harmonic constituents. Constituents with the larger amplitude have to be chosen prior to constituents with lower amplitudes. Decision trees were introduced by Forman (1977) to show Rayleigh comparison pairs along with the required record length.

The response method is another approach to tidal analysis introduced by Munk and Cartwright (1966), which in general is very closely related to the harmonic method with the major difference being the use of spherical harmonic expansion instead of a

time-harmonic expansion. In terms of accuracy the improvement using the response method rather than the harmonic approach is minimal. However, this method has not found much widespread use in tidal analysis so no mathematical explanations will be mentioned at this stage. A detailed description of the response approach can be found in Munk and Cartwright (1966).

Although both the tidal harmonic analysis and the response method meet efficiently high accuracy requirements in tidal prediction, the harmonic analysis is the by far the most common approach and will be used in this project to analyze and predict tidal records in Torres Strait.

## 1.2 Background

The Torres Strait, characterized as a continental shelf forms an oceanographic semi-barrier connecting two different ocean basins enclosing a total area of 40.000 square kilometres (Kaye1997). The Arafura Sea lies to the west on the Indian Ocean side facing the Gulf of Carpentaria and the Coral Sea lies to the east on the Pacific Ocean side facing the Gulf of Papua (Figure 1.1.). The Strait has an approximate width of 150 km with a cross-section from east to west of 20-60 km, between the islands found at its eastern and western boundaries (Kaye 1997). This area also describes a narrow, topographically complex seaway between the northwest tip of Cape York Peninsula and the south coast of Papua New Guinea. The uniqueness of the local topography stems from the extensive reef and island systems throughout the Strait (Wolanski 1994). The region also forms a biological barrier interacting with the northern limit of the Great Barrier Reef, providing a multitude of habitats for the diverse Indo-Pacific fauna (Wolanski 1994). The exceptional biodiversity and interconnectedness of species and habitats makes this region and the surrounding areas on of the most multifaceted natural systems (Wolanski 1994). The Torres Strait is estimated to be 3000 years in age, with first channels appearing 5000 – 11000 years ago.

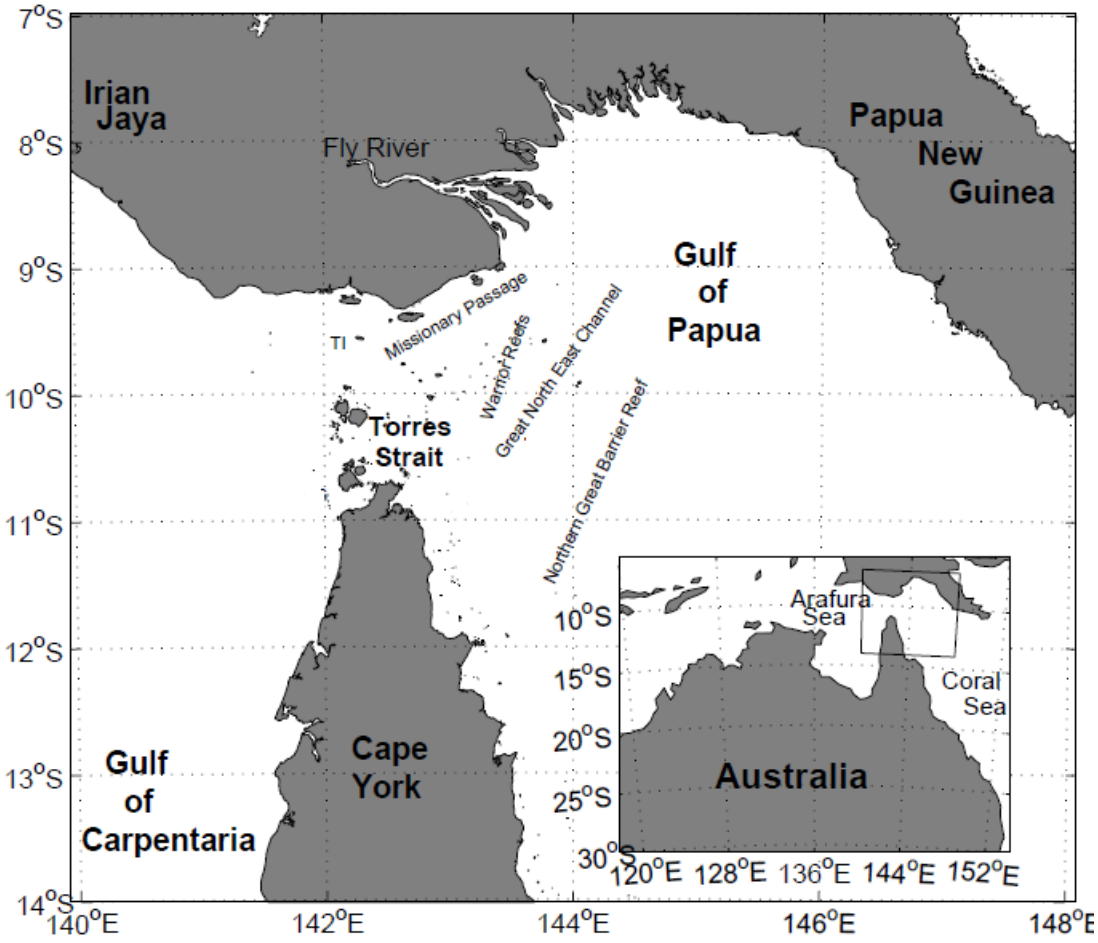


Figure 1.1: Torres Strait region. Location of Gulf of Papua and Gulf of Carpentaria is also indicated (Hemer 2003).

### 1.2.1 Topography

Numerous islands, shoals and coral reefs scatter through the Strait shaping a highly complex bathymetry. The Strait can further be divided into 3 sections each varying in depths. Figure 1.2 presents the waters of the north-western part containing a discontinuous chain of largely granitic islands with shallow depths with and limits of navigation (Daniell, J. et al. 2007). The waters west of the Strait are shallow with depths (<15m) gradually deepening westward. The northern portion of the Strait is no more than 5-10 m in depth, studded with numerous shoals and reefs (A). Isolated volcanic island and fairly flat continental shelf are found in the waters to the east with depths ranging between 15 to 20m. (C). The centre part of the Strait is dominated by scattered

coral islands with varying depths between 5-13m separated by narrow channels, typically 1-3 km wide (B) (Daniell, J. et al. 2007).

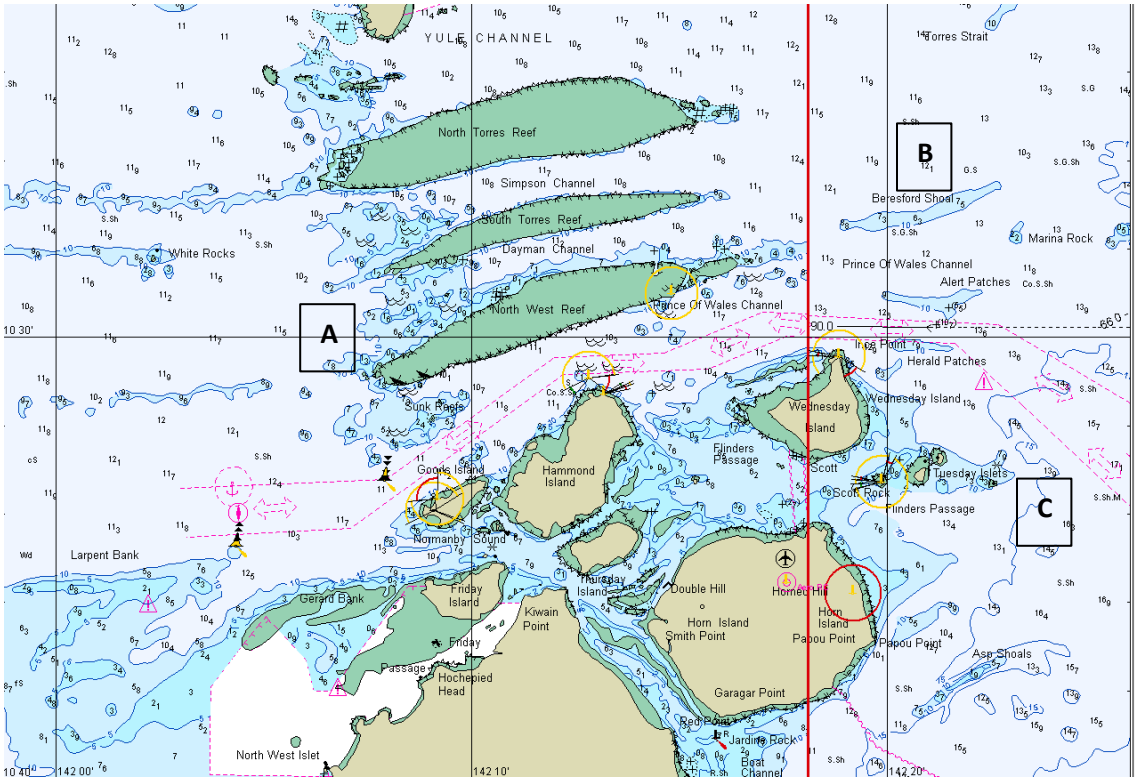


Figure 1.2: Map of the Torres Strait (Gourlay 2009). Depths are approximate and given in meters. The pink line represents the Prince of Wales Shipping Channel. Yellow circles show permanent tide gauges operated by AMSA.

The Great Barrier Reef extends over 2300 kilometres from Lady Elliot Island south of Gladstone to Papua New Guinea. To the east, the northern end of the Great Barrier Reef extends across the Strait and effectively restricts the south eastern approaches to the Strait. As a result, dense reef formations and scattered islands separate the Strait from the Coral Sea blocking oceanic swells from the Pacific Ocean. To the west, the Arafura Sea is enclosed by northern Australia and the Indonesian Archipelago, protecting the waters of Torres Strait from oceanic swells originating in the Indian Ocean (Wolanski et al 1997).

The bathymetry of the main shipping channels through the Strait has been well charted showing the shallow nature of the sea-bed, with depths varying between 6-12m.

Nonetheless, most areas remain un-navigational due to sparse bathymetric data. Knowledge gap areas of particular concern include the north east of Torres Strait, which is very complex with large reef and shoal formations, deep areas and channels as well as the north-western portion of the Strait, characterized by a very shallow bathymetry with large sand ridges and shoals, mostly uncharted and difficult to navigate.

### 1.2.2 Shipping Channels

Figure 1.3 shows the major shipping channels through the Torres Strait region. All vessels, seeking transit through the Strait from the west must pass through the Gannet or Varzin Passage to the north of Cape York continuing through the Prince of Wales Channel. The Prince of Wales Channel is a very narrow, frictional and shallow shipping channel subject to strong tidal currents (Clarke 1989). It is the main shipping channel in this region connecting the Coral Sea east of the Strait with the Gulf of Carpentaria to west of the Strait and thus forms the primary link for all shipping routes transiting the Strait, with a depth ranging from 6-12m (AMSA; Clarke 1989).

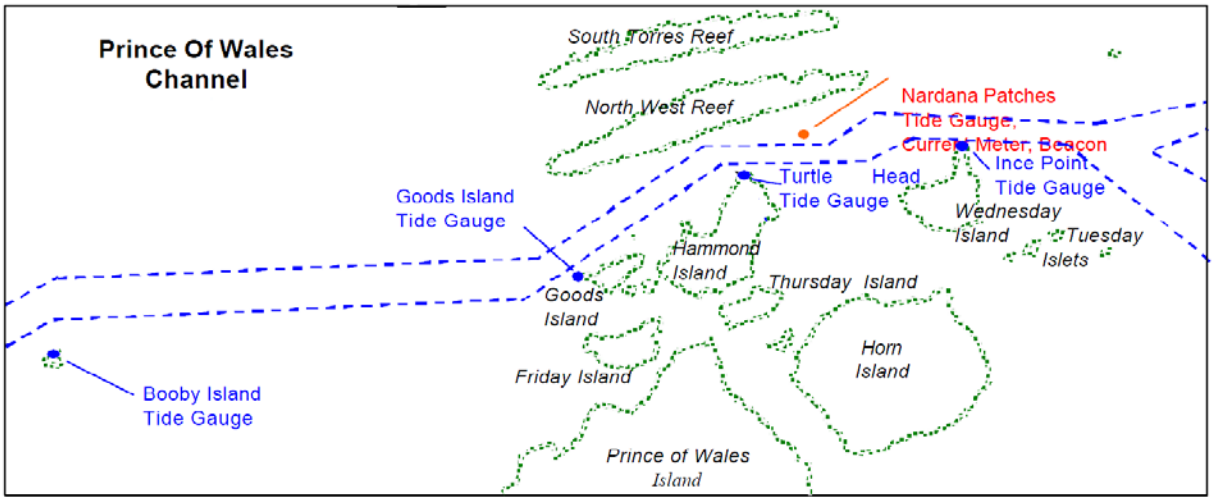


Figure 1.3: Prince of Wales Channel indicating the 5 major standard ports at Booby Island, Goods Island, Turtle Head, Nardana Patches and Ince Point.

In order to continue through the Strait, the inner and outer routes are accessible, dependent upon their intended destination (Kaye 1997). The inner route extending north-south between the Great Barrier Reef (Torres Strait) and the Queensland coast in the south (Gladstone) requires compulsory pilotage due to confined waters and high navigational difficulty. The inner route is for the most part protected from large swells and storm fronts coming from the Pacific Ocean but navigational hazards arise from the presence of numerous shoals, restricted sea room, shallow depths and reefs. The outer route is significant for ships heading to ports in the Pacific via Coral Sea and commences at the eastern limit of the Strait and continuous southwards through the Coral Sea (Kaye 1997). The outer route re-joins the Queensland coast near Sandy Cape south of Gladstone. Vessels aiming for southern Australian or New Zealand ports must navigate northward at the end of the Prince of Wales Channel, in the vicinity of Alert and Herald Patches (Clarke 1989). The outer route is of great importance for transiting vessels bound for Papua New Guinea or South Pacific Ports. However, the utmost navigational risks lie in the passage through the shallow and narrow confined waters of Torres Strait and the inner route.

### 1.2.3 Meteorology

Lying in a wet tropical region, the Torres Strait region is characterised by two distinct seasons. The wet seasons extends from December to April (southern hemisphere summer) with an average rainfall of 311 mm per months (Figure 1.5 and 1.6). From May to November the dry season (southern hemisphere winter) brings an average rainfall of 24.1 mm per months (Long et al 1997).

Prevailing wind fields are subject to strong seasonal variations with partial or complete reversal of direction. During the dry season, southeast trade winds blowing from the east and southeast dominate for 90% of the time with wind speeds seldom exceeding 30 knots (~15 m/h, Figure 1.4). The trade winds are consistent over the whole Great Barrier Reef region throughout the season. With the wet season starting, the north-westerly monsoon takes over with highly variable winds (Hemer 2003).

Winds can blow from the northeast, east and northwest. The weather then is impacted by the shift of the Inter-tropical Convergence zone into the Southern Hemisphere as well as the southwestward shift of the south Pacific Convergence Zone. Prevailing north-westerlies govern the northern Great Barrier Reef region with wind speeds of about 15 knots (~8 m/h, Figure 1.4). Even though southeast trade winds dominate the dry season; they can still be observed during wet season but with a more easterly component (Wolanski 1994). The Bureau of Meteorology maintains a weather station at Horn and Coconut Island, transmitting weather data by telemetry.

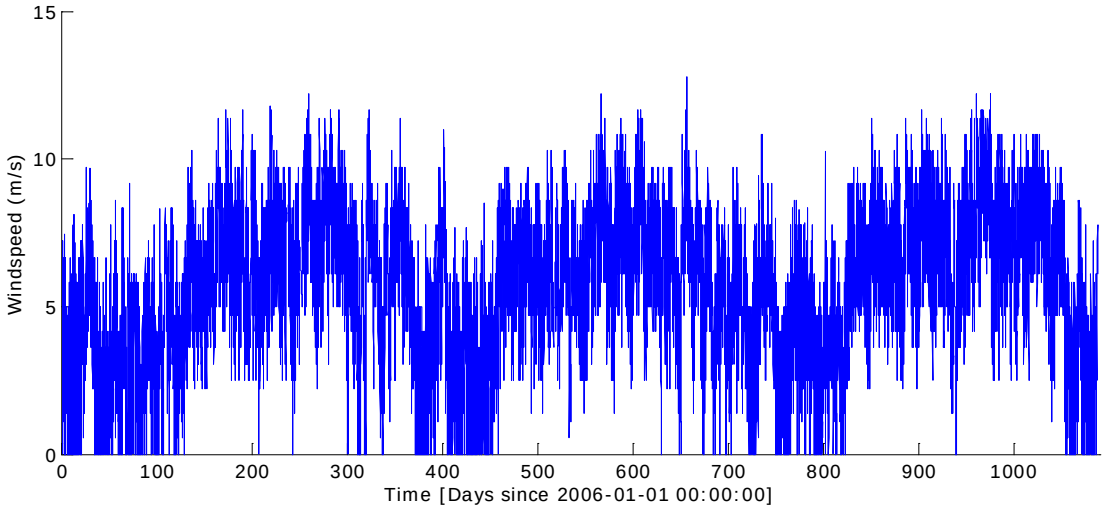


Figure 1.4: Time-series of locally observed wind speeds at Horn Island for a period of 3 years from 2006 to 2008 (10.48S; 142.29E, Bureau of Meteorology, 2009).

The tropical cyclone season spans the months from November to May, but 75% of cyclones within the Torres Strait region have been observed in January and February. The probability of cyclones north of Thursday Island has been found to be minimal (Wolanski 1994).

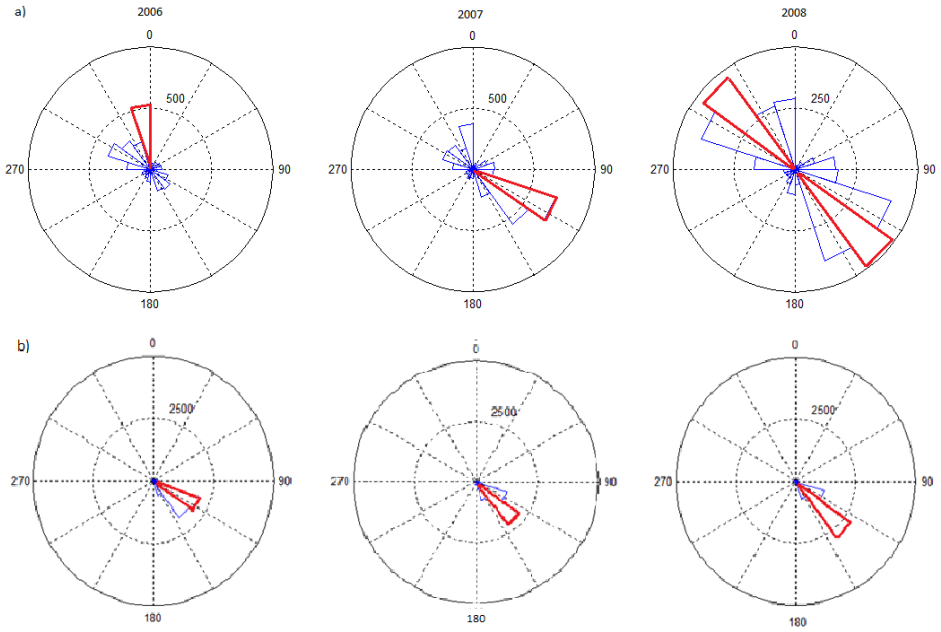


Figure 1.5: Wind roses at Horn Island (a) Prevailing wind directions in the wet monsoon (December - April) and (b) dry season (May - November) in Torres Strait. Hourly wind data was collected over a period of 3 years (2006-2008). Data has been assembled at Horn Island Airport, 4 m above ground level and 13m above sea level (Bureau of Meteorology, 2009).

### 1.2.4 Water Properties

Vertical structures of water properties found in the Strait and surrounding seas differ depending upon their location. The region within the Strait, including the northern most section of the Great Barrier Reef, is dominated by strong tidal mixing resulting in well mixed temperature and salinity profiles in the surface layer (up to 20m). The coastal waters of the Gulf of Papua are highly impacted by river runoff and prevailing wind patterns forming a fresh water plum to about 20m in depth (Wolanski 1994).Two different scenarios form the vertical structure in that region. The first scenario occurs during a period of calm wind conditions, where the freshwater plum remains stratified in salinity. The second scenario arises through a period of strong winds causing stepped salinity and temperature profiles. Water masses in the Coral Sea possess a fairly

uniform vertical profile of salinity, whereas temperature is has a stepped profile due to stratification in summer and stepped structures appearing in winter (Hemer 2003).

### 1.2.5 Fresh Water Input

Water properties in the Torres Strait region are, to a certain extent, altered by freshwater runoffs from river discharges originating in the high lands of Papua New Guinea which have an average annual rainfall of 10000 mm and an average of 3000 mm near the coast. Since Papua New Guinea lies in a wet tropical region, highest rainfall occurs throughout the wet monsoon season between December and March mainly driven by monsoonal events or nearby tropical cyclones (ENSO events lower average rainfall and river discharge). As a result, river discharges into the Gulf of Papua in the northwestern Coral Sea and the adjoining Great Barrier Reef fluctuate throughout seasons (Wolanski 1994). The Fly River, located in the Western Province of PNG meanders to the coast with a length of 800km and relative small changes in height throughout the whole course. Due to the large amount of freshwater input from the Fly River with approximately an average discharge of 7500 $m^3$ $s^{-1}$, mean temperatures of 26° C and mean salinities of about 12 psu (Saint-Cast et al 2006) it is the largest freshwater input source in this region.

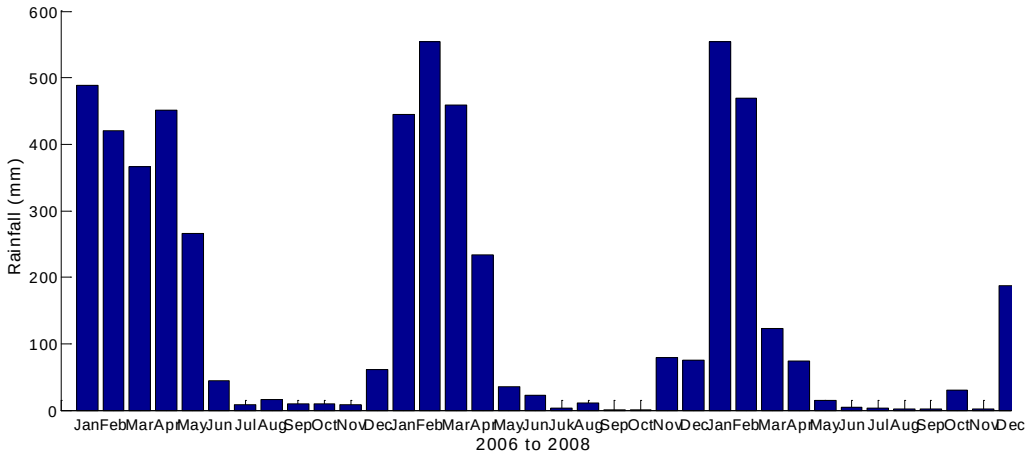


Figure 1.6: Rainfall (mm) in the highlands of Papua New Guinea from 2006 to 2008. Data was obtained for daily averages gathered at 9 am local time, PNG (Bureau of Meteorology, 2009).

The freshwater plum resulting from the Fly River runoff has been observed to propagate to Torres Strait. Intrusion events are rare and causes are mainly unknown, but on reason may be the result of sea level elevation in the Gulf of Papua and a simultaneous decrease in the Gulf of Carpentaria forced by independent large scale oceanographic processes in the Coral and Arafura Sea. The nature of these events is of time scales smaller than seasonal events (Wolanksi 1998). The impact of river runoff on sea level heights in Torres Strait is yet to be determined. But due to the complex region of the Torres Strait region combined with the unpredictable nature of rainfall and runoff events in the highlands of PNG has traditionally made data collection a difficult task to perform (Saint-Cast et al 2006).

### 1.2.6 Circulation

Even though tides and currents are known to control the physical oceanography of this region, non-tidal sea level fluctuations are to date poorly understood. The complexity of the circulation is based on the interaction of two dissimilar tidal regimes. In contrast to the tides originating from the Pacific Ocean side (Coral Sea) to the east, which are mixed but mostly semidiurnal in nature, those of the Indian Ocean (Gulf of Carpentaria) entering the Strait to the west have a diurnal pattern (Wolanski 1994). Therefore, large tidal gradients drive powerful tidal currents through the restricted areas of the Strait. As a consequence, predicted and measured tides can differ significantly in height.

The net flow through the region is strongly limited by the northern most extension of the Great Barrier Reef and numerous reef systems situated within the Strait, allowing only 29% of the semi-diurnal tidal wave to be transmitted (Wolanski 1994). The general circulation patterns in Torres Strait show a strong seasonal correlation. Throughout the time period of the dry season, southeasterly trade winds prevail with a significant westward drift of the currents. These then weaken and experience total reversal over the wet season (Saint-Cast, F. 2006). The overall net flow is westward, presenting 1% of the total Indonesian Throughflow (Long et al 1997). It

follows that the overall interaction of complex topography with wind, tides and the broad scale circulations in the adjoining Coral Sea and Gulf of Carpentaria all serve to strongly influence the circulation in the Torres Strait region (Wolanski 1994).

ENSO events (El Niño Southern Oscillation) may also impact the circulation patterns causing lower rainfall and river discharge as well as weaker occurring easterly trade winds (Long et al 1997). Even though it has been observed that the western boundary current is reinforced along the Papua New Guinea coastline facing the Solomon Sea during these events, the Coral Sea remains unaffected by these events (Wolanski 1994).

### 1.2.7 Tides in Torres Strait

The physical oceanography in Torres Strait is predominantly controlled by strong mixed tidal patterns. The geographical location forces two markedly different tidal regimes from the Coral Sea to the east and the Gulf of Carpentaria to the west through the Strait (Clarke 1989). The two tidal patterns show little to no correlation in the available tidal records and thus are out of phase with each other (Figure 1.7-1.9). As a result, large sea level gradients push powerful currents across the Strait and along the axis of the Prince of Wales Channel (Clarke 1989) leaving large differences between actual sea level measurements and predictions (Figure 1.7). Tidal currents are also strengthened by flow channelization throughout narrow passageways within the Strait and the incoherency of the different tidal regimes on either side of the Strait is a sign of the limited transmission of the tidal wave approaching the Strait from the east or the west (Wolanski et al 1988).

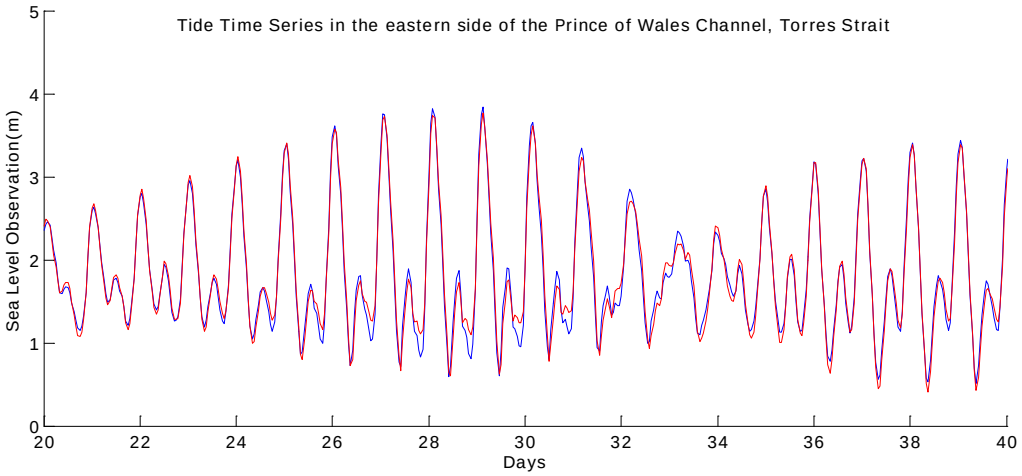


Figure 1.7: Well-correlated tidal signals within the eastern part of the POW shipping channel. Tide data (blue) obtained from Ince Point tide gauge, (red) from Nardana Patches tide gauge (r = 0.9854 ). Data spans a total of 20 days starting in February/March 2006.

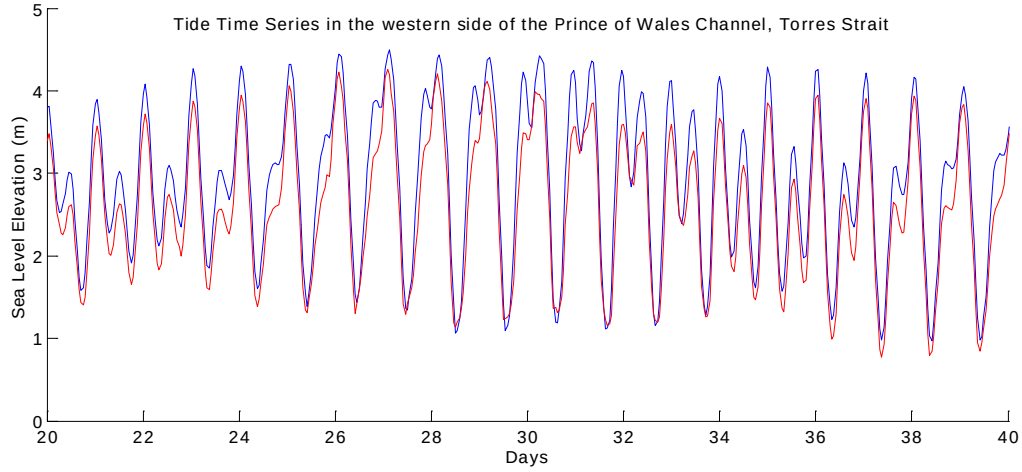


Figure 1.8: Well-correlated tidal signals within the western part of the POW shipping channel. Tide data (blue) obtained from Booby Island tide gauge, (red) from Goods Island tide gauge (r = 0.9802). Data spans a total of 20 days starting in February/March 2006.

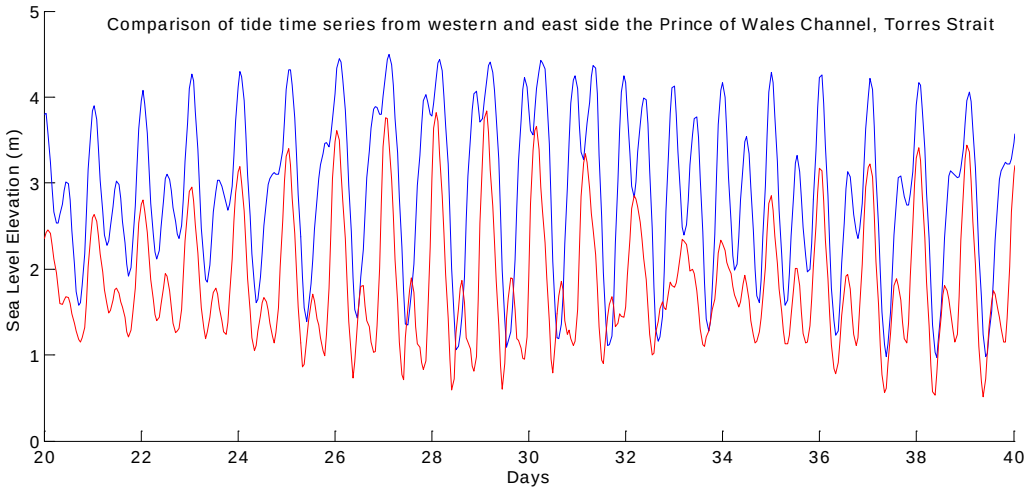


Figure 1.9: Poorly-correlated tidal signals between the eastern and western part of the POW shipping channel. Tide data (blue) obtained from Booby Island tide gauge, (red) from Ince Point tide gauge (r = 0.5834). Data spans a total of 20 days starting in February/March 2006.

### 1.2.8 Non - Tidal Sea Level Oscillations

Non-tidal sea level oscillations refer to motions which are not caused due to astronomical tidal forcing and correspond to several non-tidal parameters such as wind speed/direction, storm surges, current speed /direction and general sea level variations. In the Torres Strait region, a number of these oscillations are hypothesized to influence the overall circulation in the Strait. Observed oscillations in the Gulf of Carpentaria and Arafura Sea entering the Torres Strait region are most likely the result of passing cyclones in the Indian Ocean and Coral Sea, or by other prevailing meteorological conditions within the Gulf (Melville and Buchwald 1975). Cyclones originating in the Coral Sea have been found to propagate through the shallow waters of the Strait into the Gulf of Carpentaria. As opposite to cyclones originating east of the Strait, those who start off on the northwest Australian continental shelf will influence the circulation of the Arafura Sea-Gulf System by causing long period oscillations.

Another significant factor influencing the circulation in the Torres Strait is local forcing in the Gulf due to North-South movement of the inter-tropical convergence zone

and variations in monthly mean sea level heights (Melville and Buchwald 1975). During the period of prevailing south east trade winds, large low frequency sea level oscillations propagate on the Northern Great Barrier Reef with a maximum range of 35 cm. These low frequency oscillations are coherent with magnitudes about one tenth of the local tidal range (Wolanski 1994). But as a result of the incoherence of these oscillations on the Indian and Pacific Ocean side of the Strait, low frequency sea level slopes together with prevailing winds may force strong low-frequency currents through the Strait (Wolanski et al. 1988). All of these different mechanisms have yet to be shown to influence currents within the region of Torres Strait.

### 1.2.9 Non-Tidal and Low Frequency Current Fluctuations

An investigation of the low frequency component of the through Strait currents in the southern region of Torres Strait has concluded that over a sampling period of 5 months, these currents were for the most part governed by sea level gradients across the Strait with a significantly weaker component than the prevailing tidal component (Wolanski 1994; Hemer 2003). The swift nature of tidal induced currents together with the shallow local topography causes a strong non-linear relationship between low frequency through currents and tidal currents. Low frequency currents were observed to reverse direction from eastward to westward at periods varying from days to weeks. But low frequency sea level oscillations have been found to fluctuate significantly on either side of the Strait. Sea level observations within the western and eastern side of the southern Strait indicate low frequency sea level fluctuations up to 50 cm. These sea level fluctuations have been found not to be influenced by wind unlike low frequency currents, instead are primarily controlled by oceanic processes (Hemer 2003).

A study by Saint-Cast et al (2006) has shown that larger scale ocean circulation processes contribute to the overall surface flow, but that the reversing local wind regime is the primary driving force for monthly mean surface currents in the Strait. Wind driven surface currents reverse directions throughout the seasons with westward flows during the dry season (South East Trade Winds) and eastward flows during the wet

season (Harris, 1994; Hemer 2003). Surface currents are variable in speeds ranging from 20 to 30 cm $s^{-1}$ up to 60 cm $s^{-1}$ during dry season. Since the monsoon season is characterised by generally weaker wind speeds, resulting surface currents are of much weaker magnitude as well. Wolanski et al. (1988) found that these reversing currents may impact the magnitude of the general tidal flow by enhancing or weakening the tidal flow throughout the Strait. For oceanic budget calculations, these current vectors are of minimal significance due to the low current speeds coupled with shallow depths and negligible baroclinic motions within the Strait (Wolanski et al. 1988,; Hemer 2003).

Low frequency currents in the Gulf of Papua are controlled by several oceanic influences. These include : (i) river discharge causing strong salinity stratifications within the Gulf, (ii) currents being forced through the Great North East Channel and (iii) the influence of the Coral Sea Coastal Current operating in the northwest Coral Sea, but the overall low frequency circulation in the Gulf is weak and highly variable.

# Chapter 2. Literature Review

As discussed in the following literature review, tidal modeling in Torres Strait and other shelf regions is a complex undertaking. Contributions from Close (1918), Amin (1978), Cartwright (1968), Wolanski (1994), Saint Cast and Condie (2006), Clarke (1988), Komesaroff (1979) and Hanxing (1984) have been summarized here. In their work they have manly focused on analyzing tidal records to identify primary forcing mechanisms controlling water movement throughout the Strait.

This section commences with methods developed to predict shallow water tides and surges in areas where atmospheric parameters have the potential to significantly alter predicted water levels. A multi regression technique used by Amin in 1978 to forecast surges in Torres Strait is discussed in the beginning. It follows the explanation of a simple tidal height model including non-periodic variations i.e, short term variations in the residual time series caused by atmospheric variability. The previous work on tidal and wind analysis in Torres Strait by others is then elaborated on. Evidence regarding the influence of atmospheric forcing in the Great Barrier and Torres Strait region to impact upon water level heights is also comprehensively reviewed. Finally, a detailed overview of circulation models used to model the overall circulation in Torres Strait is described. This information is then drawn together to emphasize the importance of the current study.

## 2.1 Multiple Regression Technique to Forecast Surges

Linear and non-linear regression techniques are commonly used for forecasting surges, first introduced by Close (1918), calculating the contribution of pressure gradients to daily and monthly sea level means. Cartwright (1968) applied the response method, a technique similar to the regression technique to forecast surges on the north and west coast of Britain but with the inclusion of surges originating at nearby ports. External surges and meteorological variables have been represented as independent variables, a

technique used by the Storm Tide Warning Service in Great Britain. The response method used by Cartwright (1968), determines the effect of meteorological conditions on sea level fluctuations within the frequency domain. The major drawback to the response method is the fact that meteorological data has to be filtered before the analysis. The advantage on the other hand is the possibility of modifying the weights of frequency components in parameters. Amin (1978) suggested that the regression technique, described as the response method but applied in the time domain, has the ability to function with the input of external meteorological data as well as with sparse meteorological data.

Amin (1978) undertook a detailed field study of the effect of storm surges originating in the Arafura and the Coral Sea on the major ports in Torres Strait (Booby Island, Goods Island, Turtle Head, Frederic Island and Twin Island). Tide gauge signals spanning a time length of one year were analyzed and predicted via classic harmonic analysis using 45 astronomical and 65 shallow water constituents, subsequent residuals were then calculated. A multiple regression technique for the prediction of residual mean values using meteorological parameters was then employed.

This statistical approach to the analysis of storm surges showed that easterly winds are most dominant in the Torres Strait region with the east-west component being responsible for most surges observed. In addition, they have been found to be positive at Booby and Goods Island with prevailing westerly winds and negative with easterly winds. The results also suggested positive residual correlations between Booby Island , Goods Island, Turtle Head and Ince Point but with decreasing correlation coefficients towards the east side of the Prince of Wales Channel. Amin (1978) further elaborated that Booby Island surges are proportional to the square of the wind speed (wind stress), which enhances the importance of meteorological parameters in the prediction of tides in the western part of Torres Strait.

Results also revealed that meteorological tides (non-periodic, wind induced flows) are not fully transmitted across the Prince of Wales Channel. The here introduced multiple regression technique is also used in this project for its simplicity and self-applicable character.

## 2.2 Review of Previous Work on Predicting Shallow Water Tides

Hanxing (1984) showed that for shallow ports impacted by non-periodic water level fluctuations such as wind and pressure variations, the addition of a Weather Chart Predicting Method to account for the post inclusion of non-periodic variability to the regular harmonic analysis reaches a higher accuracy outcome for shallow ports than predicting water levels with harmonic constants alone. This method is based on a correlation between specific weather conditions and water levels, which can then be used as a reference point to apply corrections for future water levels with similar prevailing atmospheric conditions. It follows that a recurring character of non-periodic variations of water levels associated with specific atmospheric conditions is assumed. Thus, a detailed analysis of historical atmospheric conditions and the associated water levels would allow to correct future water levels based on prevailing weather conditions. The combination of harmonic analysis to determine the harmonic constituents and the analysis of atmospheric conditions to allow for non-periodic variability has shown excellent results in the shallow Changjiang Esturary, China. This method is applicable to shallow ports sensitive to atmospheric variability and thus the basic idea of this method will be used to analyze large amplitudes in the residual time series at Booby Island, Torres Strait.

Clarke (1988) applied a frictional channel flow theory to flow in the Price of Wales Channel to identify characteristics of tidal currents. The study showed that tidal currents in the Price of Wales Channel are governed by the bottom friction and the sea level slope. Findings also indicated that present tidal current predictions do not take varying interannual or mean flows into account nor meteorologically driven surges which strongly interfere with tidal currents as shown by Amin (1979).

Wolanski et al., (1988) performed a five months field study of the current flow through the Torres Strait region with a detailed numerical analysis of sea level and current data obtained from several locations throughout the Strait and others deployed close to the Coral and Arafura Sea. Sea level and current data were analyzed using

classic harmonic analysis as described by Foreman (1978) to determine the harmonic constants, which then were used to produce predicted sea level and current sea levels. The residual time series was defined as the difference of the observed and the predicted time series. To determine non-periodic sea level oscillations (meteorological tides), further analysis on the residual time series was performed. To separate low frequency oscillations from the residual time series a moving average filter (Godin 1972) was applied. High frequency oscillations were defined as the difference between the low frequency and the residual time series. Results clearly indicated that most tidal energy lies within the semidiurnal and diurnal tidal signals.

They further showed that tides and low frequency sea level oscillations are highly incoherent on either side of the Strait and that low frequency currents propagating through the Strait reverse directions at varying periods. Wolanski (1988) hypothesized that the strong low frequency currents observed in Torres Strait are the result of the low frequency sea level slope through the Strait coupled with local wind stress. The results were inconclusive due to the limited number of current meters to adequately identify the motions. Although the approach by Wolanksi et al., (1988) is able to reproduce a number of observations of tidal and low-frequency motions, it was not designed to be a predictive tool using prevailing meteorological conditions.

Wolanksi and Thomson (1984) carried out a five month intensive field and numerical study on atmospheric conditions and tides in the northern Great Barrier Reef Continental Shelf during the wet season. A weather station, several tide gauges and current meters were deployed in the far northern Great Barrier Reef. To separate periodic from non-periodic oscillations, tidal harmonic analysis was used to determine harmonic constituents followed by the application of high and low pass filtering techniques. The prevailing wind direction throughout the deployment was north-westward with highly variable wind velocities. Further results indicated that net currents were small in magnitude ($<0.1 ms^{-1}$) with reversing directions at varying periods.

## 2.3 Method of Tidal Windowing in Torres Strait

Tides and tidal flows play a key role in developing navigational aids to minimize the possibility of groundings and timing errors of vessels in shallow regions. Although not large by world standards, the number of commercial and industrial vessels (~ 3000 annually) passing through the Strait is not insubstantial. Today, all vessels over 70 m in length require pilotage through the complex reef systems in Torres Strait with the minimum Under Keel Clearance being set between 1 m up to 11.9 m and 10 % of draught for vessels having a draught of 11.9 m – 12.2 m.

Komesaroff (1979) showed through the application of a tidal window technique the correlations between ship draught, speed, direction, seasonality and the resulting Strait closures. The method of tidal window is based on the superimposition of the tide contour onto one diagram and the time shifting by the steaming time for each leg , where contour lines join points in time which have the same minimum tide height.

The simplified model implies that season and a ships specific draught are responsible for most Strait closures throughout the year. In 1979, ships trans-passing through the Strait had a draught limitation of 11.89 m with a minimum underkeel clearance of 1 m, in which case seasonality is less critical since Strait closures can be overcome by minor speed adjustments. However, deeper draughts have been shown to result in more Strait closures. East – bound vessels travelling with a speed of 9 km/h the Torres Strait encounter a total of 51 days of Strait closure. With an increased draught to 12.19 m the number of days of total closure increases rapidly to 223 days. A further increase to 12.5 in draught means a closure time of 339 days. Furthermore, it has been demonstrated that Booby Island is the most critical port in the Strait in regards to draught limitations, speed and Strait availability.

## 2.4 Tide and Circulation Models in Torres Strait

With the launch of the altimetry satellite Jason 1 and the pioneering TOPEX/POSEIDON satellite altimetry, knowledge of the dynamics of ocean circulation and deep oceanic tides has greatly improved on a global scale. Although deep oceanic tides can now be modeled with high accuracy, the complex nature of shallow water tides still causes great problems in the application of these models. The major difficulty in modeling shallow water tides is the implementation of bathymetry in the model and thus, global ocean tide models fail to adequately model the local resonances caused by shallow water dynamics.

A number of hydrodynamic models have previously been applied for simulating tidal and circulation dynamics in the Torres Strait region. As these models presented an overall improvement in more realistic simulations, relative coarse resolutions of the models coupled with the geographic complexity of the region limited the successful outcome of the simulations (Saint-Cast and Condie 2006).

Chittleborough (2007) discussed the development of the Australian Continental Shelf Model at the National Tidal Centre Australia. As general global tidal models are mainly empirical models altered fit to sea surface observations, the Australian Continental Shelf Model provides higher resolution tidal modeling for the Australian continental shelf region. The model enables the simulation of tides and meteorologically-driven motions over large areas. It also allows for the determination of present tidal constituents over the entire Australian continental shelf with a resolution of 5 minutes in latitude and longitude. Even though this model gives an improvement in regards to bathymetric resolution, the demand for higher resolution modeling continues.

Frederic Saint-Cast and Scott Condie (2006) applied the Sparse Hydrodynamic Ocean Code (SHOC) with fine scale resolution to model the circulation in Torres Strait using realistic atmospheric forcing mechanisms such as winds, tides and large scale regional circulation for a total of eight years. This model has previously been used for the Torres Strait region but with a coarse scale resolution and non-realistic atmospheric forcing mechanisms.

The data suggested that wind stress is mainly responsible for longer term through Strait transport. A net westward flux of water from the Coral to the Arafura Sea has been detected during periods of prevailing southeasterly trade winds. Tidal signals through the Strait show little to no correlation confirming the assumption that tidal dynamics in the Strait are the result of the interference of the different tidal regimes on either side of the Strait. The amplitude/phase of the tidal signal changes rapidly throughout the Strait. Model results were shown to be generally realistic, but with the need for further improvement regarding the inclusion of higher resolution winds to capture the effect of sea breezes on the circulation.

## 2.5 Conclusion and Justification of the current study

The preceding discussion has highlighted the lack and therefore the resulting need of tidal modeling/prediction methods in Torres Strait using prevailing atmospheric conditions. Overall, wind dynamics have been shown to potentially affect sea levels and currents throughout the Torres Strait region. These non-periodic changes in sea level, which have not been able to be predicted, will significantly lower the accuracy of tidal models.

# Chapter 3. Methodology

### 3.1 Sea level Data

Tide gauge readings for a period of 3 consecutive years from January 1 of 2006 to December 31 of 2008 were obtained from 5 standard ports located within the vicinity of the Prince of Wales Channel, Torres Strait. Standard ports, operated by the Australian Maritime Safety Authority are provided with daily predictions of high and low waters based on lowest astronomical tide datum. Sea level observations were recorded in hourly intervals. The geographical positions of the stations are shown in Figure 3.1. Several malfunctions of the tide gauges at each station caused gabs in sea level measurements (Table 3.1).

Tide Gauge Locations and Error Readings for 3 Year Sampling Period

| Station Name (west-east) | Position (WGS 84) | Hour | Days (rounded) |
|---|---|---|---|
| (1) Booby Island | 10° 36’09’’S<br>141° 54’36’’E | 368 | 15 |
| (2) Goods Island | 10° 33’ 53’’S<br>142° 08’44’’E | 75 | 3 |
| (3) Turtle Head | 10° 31’ 14’’S<br>142° 12’47’’E | 470 | 20 |
| (4) Nardana Patches | 10° 30’ 17’’S<br>142° 14’38’’E | 108 | 4 |
| (5) Ince Point | 10° 30’ 51’’S<br>142° 18’17’’E | 202 | 8 |
| (6) Horn Island | 10° 35’ 40’’S<br>142° 17’24’’E | - | - |

Table 3.1: Error readings of observed sea levels due to unknown malfunctions of tide gauges. Gabs occurred randomly distributed over the spanning time period. Booby Island tide gauge shows error readings for 7 consecutive days in 2006. Turtle Head has the longest gab with 14 days in 2007. Remaining gabs are of shorter lengths.

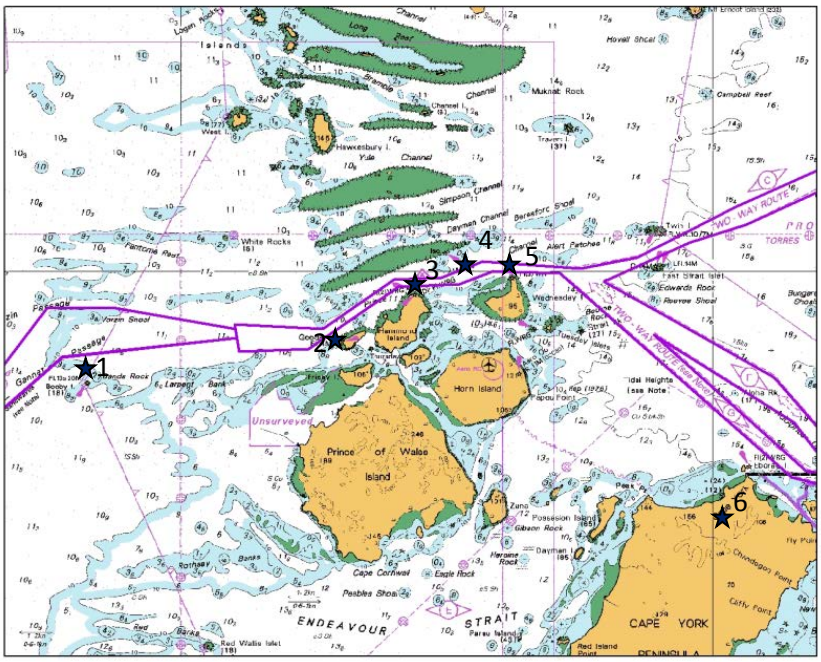


Fig 3.1: Tide Gauges and Weather Station (6) along the Prince of Wales Channel, Torres Strait. Purple lines indicate the inner route, outer route and Great North East Channel.

### 3.1.1 Meteorological Data

Wind and atmospheric pressure data were obtained from the weather station located at Horn Island Airport (Bureau of Meteorology, 2009). Wind speed and direction were recorded in hourly intervals for a total of 1095 consecutive days from 2006 to 2008. Significant weather changes were observed with shortened intervals between measurements. Thus, in order to adopt a uniform timing system of 1-hour observations for wind/pressure and tidal data, 1-D interpolation of data was performed. The meteorological convention was used for the wind.

### 3.1.2 Analysis and Interpretation

The obtained data sets were subject to several data management procedures such as the finding and removal of data gabs, interpretation of unusual spikes and the conversion to applicable formats. Data formatting, visualization and analysis was performed using Microsoft Excel/Word and Matlab Simulink. The extraction of tidal frequencies, needed for the reconstruction of the original tidal signal was performed using Harmonic Analysis (Hamels Method). Residual time series were computed by subtracting the astronomical predicted tides from the measured tidal signal. The adequate resolution of tidal constituents is dependent on two variables, record length and local bathymetry. Due to the relative short record length of 3 consecutive years and the complexity of the local bathymetry, residual time series from AMSA are used for comparison and final prediction purposes. AMSA utilizes 24 years of previous tidal records to resolve a total of 112 harmonic constituents which are then further used for tidal predictions. Statistical analysis is used to investigate the role of meteorological conditions in the development of residual time series. A regression technique to forecast tidal residuals in Torres Strait is applied.

| Tida Gauge Station | Constituents (AMSA) | Constituents (Ribbat) | Days of Data (AMSA) | Days of Data (Ribbat) |
|---|---|---|---|---|
| Booby Island | | | 5981 | 1079 |
| Goods Island | | | 6098 | 1092 |
| Turtle Head | 112 | 128 | 5926 | 1075 |
| Nardana Patches | | | 943 | 1090 |
| Ince Point | | | 6129 | 1086 |

Table 3.2: Number of tidal constituents and time in days used to obtain residual time series for the 5 stations along the Prince of Wales Channel. Harmonic analysis carried out by AMSA and Ribbat.

## 3.2 Tidal Harmonic Analysis

In shallow regions like Torres Strait, the distortion of the astronomical tidal signal by shallow water effects is a dominant. Following Munk and Catrwright (1966), additional constituents representing sums and differences of already known frequencies can be introduced to count for some of the shallow water effects. These individual component parts are stimulated by different and often independent physical processes. Thus, a fundamental concept of tidal analysis is the separation of tidal from non-tidal energies. Here, tidal harmonic analysis using Hamels Method, a least squares solution (Magori 2008) is performed to separate tidal from non-tidal components to determine tidal constituents for sea level data. Constituents are chosen according to the Rayleigh Criterion (Godin 1972). Different sets of constituents are fitted to obtain best results. The performances of these sets are shown in Figure 4.7 and 4.8. The constituents then are used to recreate the time series of tidal observed sea levels.

As suggested by Amin (1978), any sea level measurement $Z_t$, defined as the deviation of observed sea level from the mean sea level can be expressed as

$$Z_t = Z_t^{(T)} + S_t + N_t \quad (1)$$

where $t$ is the time,

$Z_t^{(T)}$ is the tidal component,

$S_t$ is the non-tidal component (meteorological residuals),

$N_t$ is the residual variation independent of present forces

The tidal component $Z_t^{(T)}$, is predicted as follows. Given the time series of observed sea level data $Z_t$ of $N$ data points, where $N$ is the number of samples taken at the standard ports, the tidal periodic motion can be represented as a combination of sine and cosine functions.

$$Z_t^{(T)} = \sum_j A_j sin(2\pi f_j\, t) + \sum_j B_j cos(2\pi f_j\, t) \quad (2)$$

To solve for the unknown coefficients $A_j$ and $B_j$ , which are obtained for the given frequencies $\omega_j$, where $\omega_j = 2\pi f_j$ the summed square of the residuals is minimized. Here the residual for the jth data point ri is defined as the difference between the assumed function and the given time series $Z_n$.

$$f(A_j, B_j) = \sum_{n=1}^{N} \left( z_n - \sum_j A_j \, sin(\omega_j t_n) + \sum_j B_j \cos(\omega_j t_n) \right)^2 \quad (3)$$

It follows that if N > j, where j is the number of unknowns, the system of equations then becomes over determined.

The coefficients can then be determined by differentiating $f(A_j, B_j)$ with respect to each parameter subsequently setting the result equal to zero.

$$\frac{\partial f}{\partial A_i} = 0, \qquad i = 1, \dots, j \quad (4)$$

And

$$\frac{\partial f}{\partial B_i} = 0, \qquad i = 1, \dots, j \quad (5)$$

Where

$$\frac{\partial f}{\partial A_i} = -2 \sum_{n=1}^{N} cos(\omega_i t_n) \left( z_t - \sum_j A_j \, sin(\omega_j t_n) - \sum_j B_j \cos(\omega_j t_n) \right) = 0 \quad (6)$$

And simultaneously for

$$\frac{\partial f}{\partial B_i} = -2 \sum_{n=1}^{N} sin(\omega_i t_n) \left( z_t - \sum_j A_j \, sin(\omega_j t_n) + \sum_j B_j \cos(\omega_j t_n) \right) = 0 \quad (7)$$

Now we can rearrange the above equations in the following form, yielding

$$\sum_j A_j \sum_{n=1}^{N} sin(\omega_j\, t_n)\, cos(\omega_j t_n) + \sum_j B_j \sum_{n=1}^{N} sin(\omega_i t_n)\, sin(\omega_j t_n) = \sum_{n=1}^{N} Z_n sin(\omega_i\, t_n) \quad (8)$$

$$\sum_j A_j \sum_{n=1}^{N} cos(\omega_j\, t_n)\, cos(\omega_j t_n) + \sum_j B_j \sum_{n=1}^{N} cos(\omega_i t_n)\, sin(\omega_j t_n) = \sum_{n=1}^{N} Z_n sin(\omega_i\, t_n) \quad (9)$$

These two equations can be simplified by introducing the following notation (Magori 2008) let

$C_{in} = cos(\omega_i t_n)$ and

$S_{jn} = sin(\omega_j t_n)$

So equations 8 becomes

$$\sum_j A_j\, S_{jn} C_{jn} + \sum_j B_j\, S_{in} C_{jn} = \sum_n Z_n S_{in} \quad (10)$$

And similarly for equation 9

$$\sum_j A_j\, C_{jn} C_{jn} + \sum_j B_j\, C_{in} S_{jn} = \sum_n Z_n S_{in} \quad (11)$$

Leaving us with a system of 2j equations with 2j unknowns, namely $A_i$ through $A_j$ and similarly $B_i$ through $B_j$. It follows that the linear least squares solution can then be expressed using the following matrix symbols

$$[A] = [SSX]^{-1}[SXY] \quad (12)$$

A detailed approach to this least squares fit can be found in Magori (2008).

To perform further analysis on the residuals existing gabs in the time series have to be interpolated. In this case an interpolation method commonly used in communication systems will be applied to the residual time series of Booby Island. This interpolation method was introduced by Vaseghi and Rayner in 1990 for the removal of impulsive disturbances from noisy speech and musical signals. The signal samples that are dominated by impulsive noise levels are discarded and interpolated. The interpolation method produces a least squared error estimate of the missing samples using data samples in close proximity of the missing block and an estimate of the LPC model of the signal. The accuracy of the interpolation depends on the performance of the interpolation algorithm which strongly relies on gab length and occurrence frequency. Hence, high order algorithms require sufficient long time periods between existing gabs to adequately interpolate the missing or false signal. Details can be found in Vaseghi et al 1990.

## 3.3 Regression Technique

After the tidal component $Z_t^{(T)}$ has been determined and interpolated to hourly intervals, equation (1) can be rewritten as

$$R_t = Z_t - Z_t^{(T)} = S_t + N_t \quad (13)$$

where $R_t$ is the sum of the non-tidal component ($S_t$) and the uncorrelated residual noise ($N_t$). The prediction of surges and sea level variations normally requires the use of complex numerical models. Here, a regression method is applied first introduced by Doodsen (1924) and most recently by Amin (1978) to develop a system for forecasting residual sea level heights using meteorological data. Following Amin's approach, changes in sea level heights or surges induced by meteorological forcing mechanisms can be expressed in a regression equation as

$$S_t = \alpha_1\left(X_t^{(1)} - \bar{X}^{(1)}\right) + \alpha_2\left(X_t^{(2)} - \bar{X}^{(2)}\right) \dots \alpha_m\left(X_t^{(m)} - \bar{X}^{(m)}\right) \quad (14)$$

where $X_t^{(1)}$, $X_t^{(2)}$ are specified meteorological parameters such as wind or barometric pressure, $\alpha_1$, $\alpha_2$ are regression coefficients for the input parameters and $\bar{X}^{(1)}$, $\bar{X}^{(2)}$ are the averages of $X_t^{(1)}$, $X_t^{(2)}$. The time interval selected to cover the appropriate surge event/ sea level variation, is usually defined as the period of conditions enhancing the generation of a surge. In this study, it is aimed to approximate the residual sea level height in a time span of several years with the main focus being the west wind component, suggested to generate large parts of the residual seal level detected in the vicinity of the Prince of Wales Channel.

Equation (14) represents a simple linear equation with solutions only giving linear components of the surge/residuals. It follows that an immediate response of sea level is assumed. However, the oceanic response to external perturbations is not instantaneous in time (Amin 1978). Various variables play an important role for the adjustment of sea level height to meteorological forcing mechanisms. Such variables include spatial variation, local topography, wind speed, duration of impact and direction. Thus, various time lags $\tau$ can be included in the analysis to allow for time delays between meteorological events its oceanic response.

$$S_t = \alpha_1\left(X_{t-\tau_1}^{(1)} - \bar{X}^{(1)}\right) + \alpha_2\left(X_{t-\tau_2}^{(2)} - \bar{X}^{(2)}\right) \dots \alpha_m\left(X_{t-\tau_m}^{(m)} - \bar{X}^{(m)}\right) \quad (15)$$

By combining equation (1) and (15) we obtain an equation for the residual water level

$$R_t = \alpha_1\left(X_{t-\tau_1}^{(1)} - \bar{X}^{(1)}\right) + \alpha_2\left(X_{t-\tau_2}^{(2)} - \bar{X}^{(2)}\right) \dots \alpha_m\left(X_{t-\tau_m}^{(m)} - \bar{X}^{(m)}\right) + N_t \quad (16)$$

And by neglecting the noise term $N_t$ we have

$$R_t = S_t$$

It follows that by neglecting the noise term, the estimate of $R_t$ should be roughly the measured surge or sea level elevation at a particular location.

For the time subset t = [1,N], equation (1) gives a terminated system which is solved using the least squares approach, such that $< (\boldsymbol{R} - \boldsymbol{S})^{\mathbf{2}} >$ is minimum. The solution will consist of a set of N+1 equations such that XA = R and A = X \ R

$$\begin{bmatrix} R_1 \\ R_2 \\ R_3 \\ R_n \end{bmatrix} = \begin{bmatrix} 1 & X_{\tau_1}^{(1)} & X_{\tau_2}^{(2)} & \cdots & X_{\tau_m}^{(m)} \\ 1 & X_{\tau_1-1}^{(1)} & X_{\tau_2-1}^{(2)} & \cdots & X_{\tau_m-2}^{(m)} \\ 1 & X_{\tau_1-2}^{(1)} & X_{\tau_2-2}^{(2)} & \cdots & X_{\tau_m-1}^{(m)} \\ 1 & X_{\tau_1-N}^{(1)} & X_{\tau_2-N}^{(2)} & \cdots & X_{\tau_m-N}^{(m)} \end{bmatrix} \times \begin{bmatrix} \alpha_1 \\ \alpha_2 \\ \alpha_3 \\ \alpha_m \end{bmatrix} for\ N > m \qquad (16)$$

The inclusion of all meteorological parameters as well as the amount of uncorrelated noise level will determine the overall quality of the estimate of A. In addition, since input parameters differ in units such as wind speed and barometric pressure, they have been converted to dimensionless quantities through normalization with respect to their standard deviations (std), i.e

$$\frac{R_t}{S_{std}} = \alpha_1 \left( \frac{X_{t-\tau_1}^{(1)}}{S_{stdX1}} \right) + \alpha_2 \left( \frac{X_{t-\tau_2}^{(2)}}{S_{stdX2}} \right) \ldots \alpha_m \left( \frac{X_{t-\tau_m}^{(m)}}{S_{stdXm}} \right) \qquad (17)$$

Thus, the final estimate of the residual tide /surge level resulting from the above calculation is expressed as

$$\tilde{R}_t = \alpha_1 \left( X_{t-\tau_1}^{(1)} \right) + \alpha_2 \left( X_{t-\tau_2}^{(2)} \right) \ldots \alpha_m \left( X_{t-\tau_m}^{(m)} \right) \qquad (18)$$

Where $\tilde{R}_t$ denotes the estimate of $R_t$.

The system for forecasting tidal residuals used above assumes that the non-periodic residual water level under certain weather condition in the future is somehow a repetition of the non-periodical water level variations under similar weather conditions in history. Therefore, if a correlation between particular meteorological conditions of

tidal data with the corresponding residuals at Booby Island, Goods Island, Turtle Head, Nardana Patches and Ince Point is found, the correlation is then used as a basis on which corrections under the similar meteorological conditions in the future could be made on the water level prediction at these stations.

Since for prediction purposes of these tidal residuals, main considerations are given to the factors of meteorology, cross-correlation functions of tidal residuals (Booby Island, Goods Island, Turtle Head, Nardana Patches, Ince Point) with (atmospheric pressure (p) and west wind (u) were applied to find the relationship amongst them (Figure 4.14 and 4.15). Table 4.3 indicates a pronounced correlation between westerly winds and tidal residuals in the case of Booby Island located at the most western point of the Prince of Wales Channel. It proposes an almost immediate response to westerly winds and might be the predominant contribution to the generation of non-tidal surges. Thus, the analysis is concentrated on Booby Island data from AMSA. Harmonic analysis using 128 constituents and a 3 year data set, a linear correlation factor of 0.4075 for the west wind and -0.2509 for Atmospheric pressure was found.

In order to determine frequencies which initially were not included in the harmonic analysis, a Butterworth low-pass filter is applied to the meteorological and reconstructed residual time series (Figure 4.11-4.13). Correlation coefficients are shown in Table 4.4.

As mentioned earlier, the response of the sea level to spatially varying meteorological conditions is most likely not instantaneous, but rather delayed in time. In order to determine the best solution of equation (18) to fit the residuals at Booby Island, the system (16) is solved using a variety of time lags. In order to quantify how well the prediction method worked, correlation coefficients were calculated between Booby Island residuals (AMSA) and each of the corresponding forecasts (Figure 4.16 – 4.21)

It has been found that the most suitable forecasting time lag on the principal parameters ($u^2$, wind stress and $p$, atmospheric pressure) has been established to be an average of the previous 24 hours of weather data resulting in a linear correlation of

0.6294 (Figure 4.22) So for the best estimation of the system at Booby Island, equation (18) is assumed

$$R_t = 0.3020\overline{u^2 24} + 0.0740u^2 - 0.2014\overline{p24} \quad (19)$$

where $u^2$ is the west component of the wind stress at Horn Island , $\overline{u^2 24}$ is the average of the previous 24 hours of wind stress at Horn Island and $\overline{p24}$ is the average of the previous 24 hours of atmospheric pressure at Horn Island. Consequently, in order to utilize equation (19) for predicting residual behavior in advance, previous meteorological data and future forecasts are necessary.

# Chapter 4. Results

## 4.1 Tidal records (AMSA)

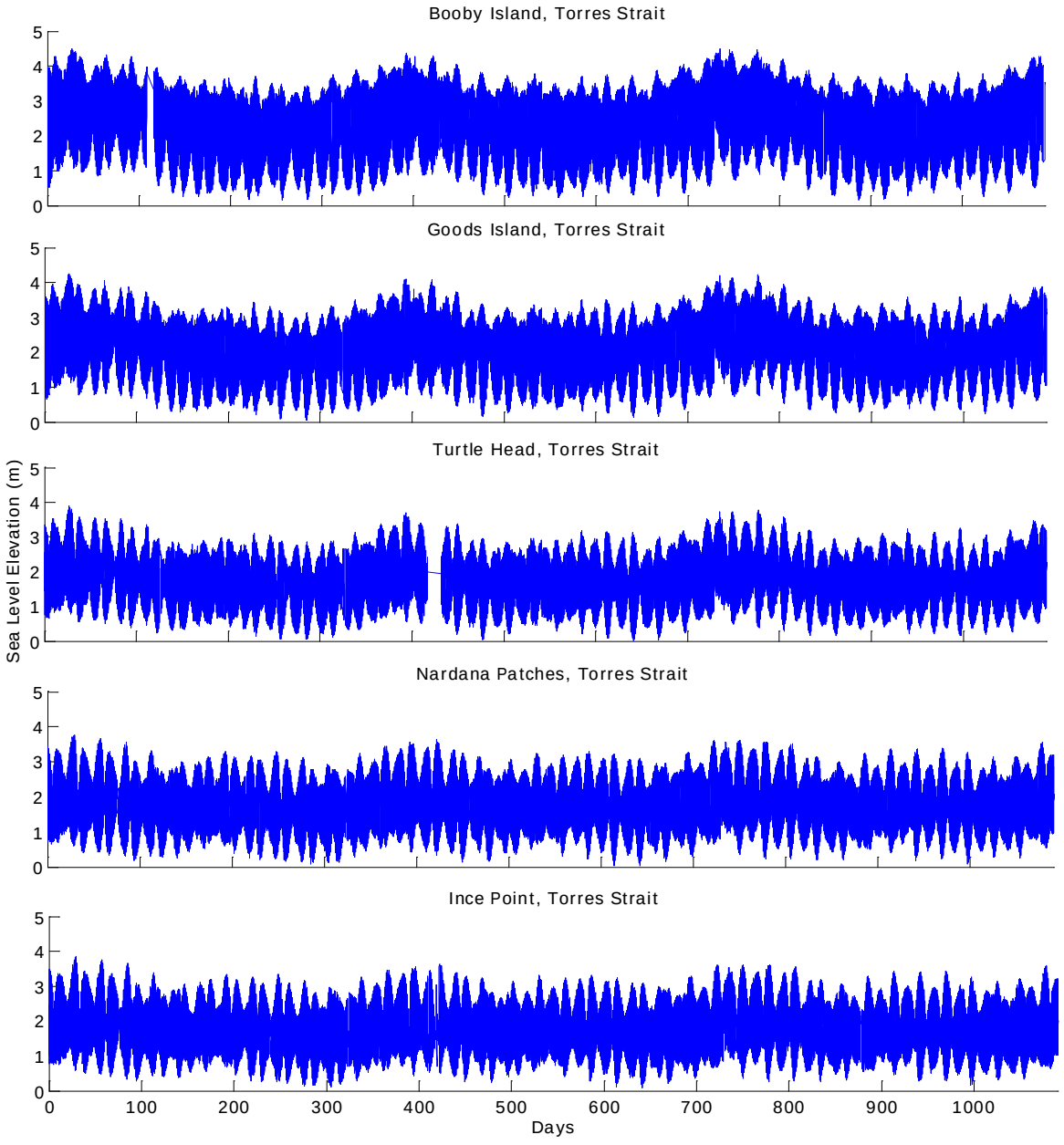


Figure 4.1: Five standard ports tide gauge time series showing measured sea level data from 2006 to 2008. Raw data obtained from the Australian Maritime Safety Authority, 2009.

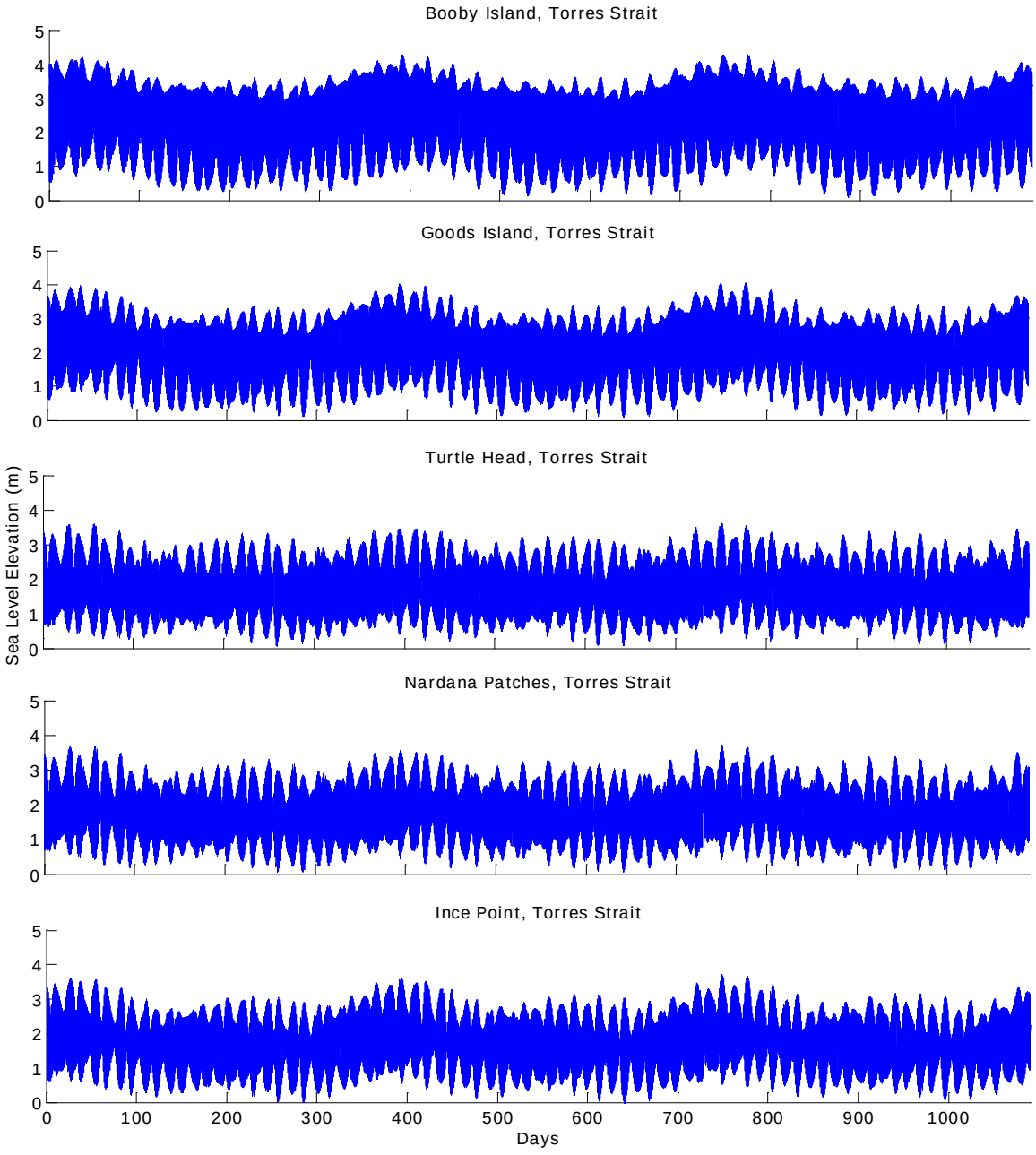


Figure 4.2: Predicted tide height (AMSA 2009) using 112 tidal constituents and 24 year tidal data. Prediction spans from January 1, 2006 to 2008.

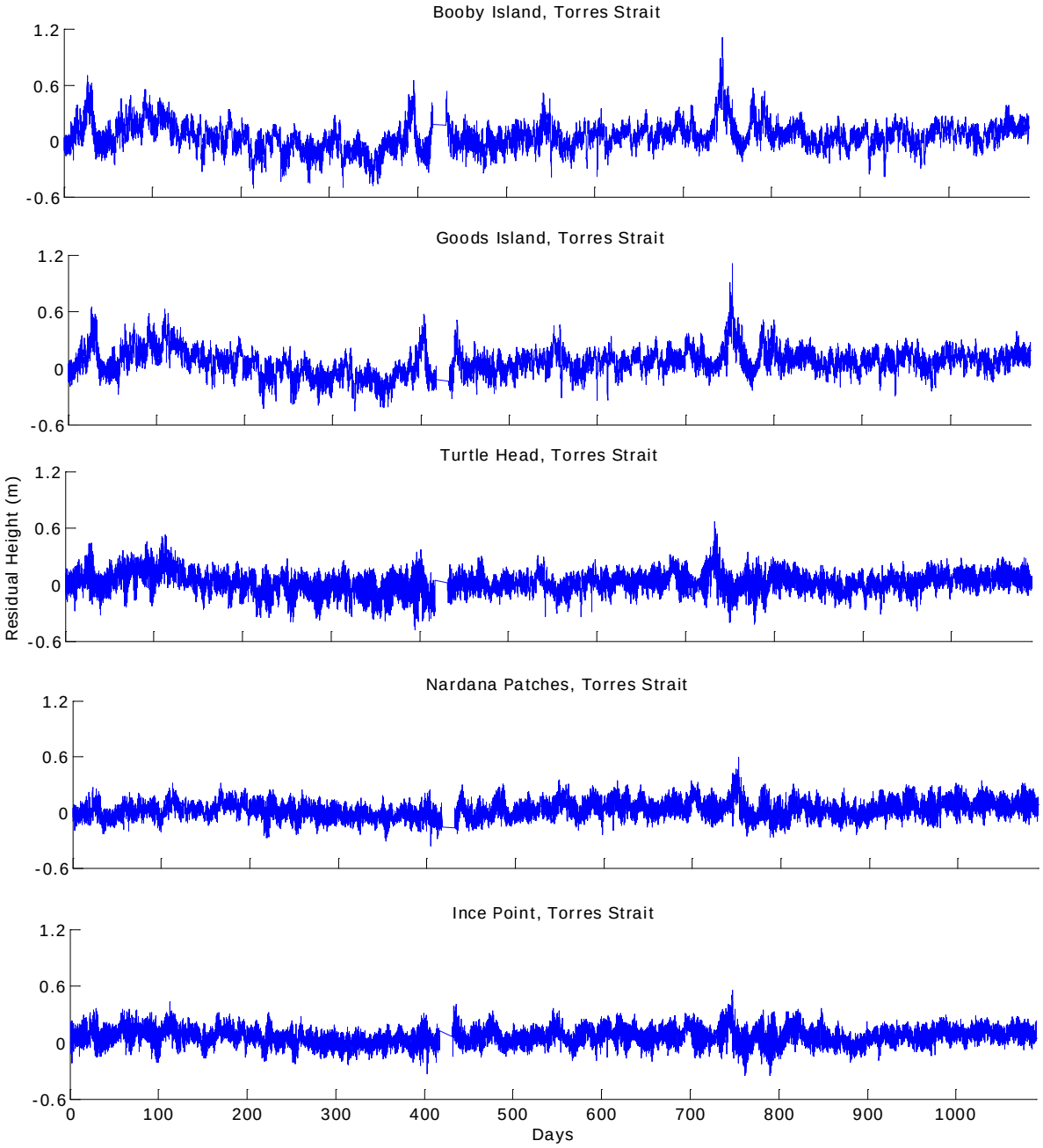


Figure 4.3: Residual tide height obtained from subtracting observed from predicted tide height. (AMSA 2009), spanning time range from January 1, 2006 to 2008.

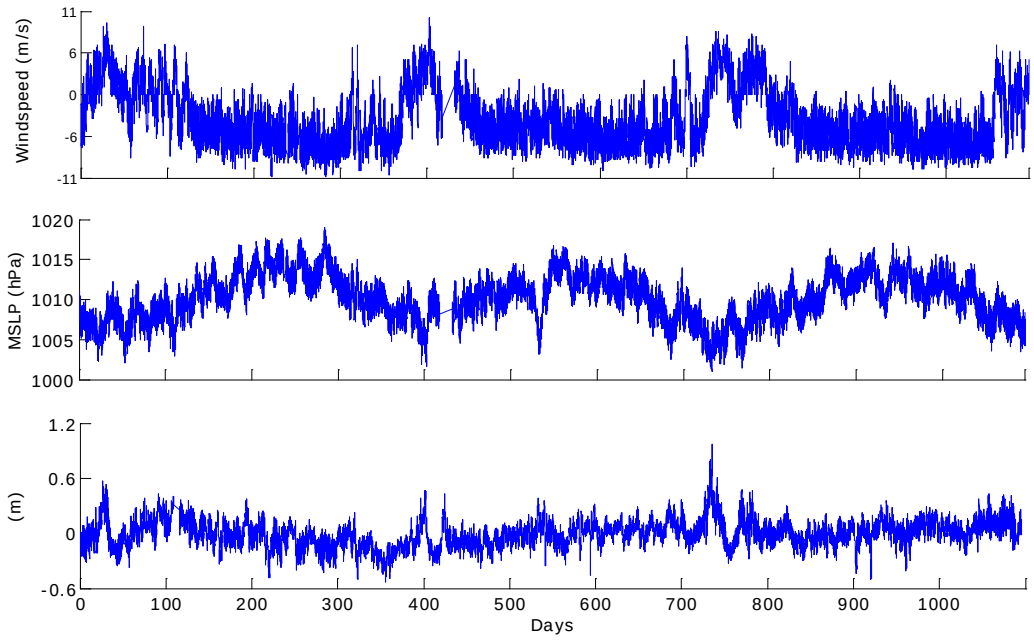


Figure 4.4: Time series plots showing (top to bottom) west wind speed, atmospheric pressure and observed tidal residual at Booby Island. Time is given as from January 1, 2006-2008.

## 4.2 Data Interpolation

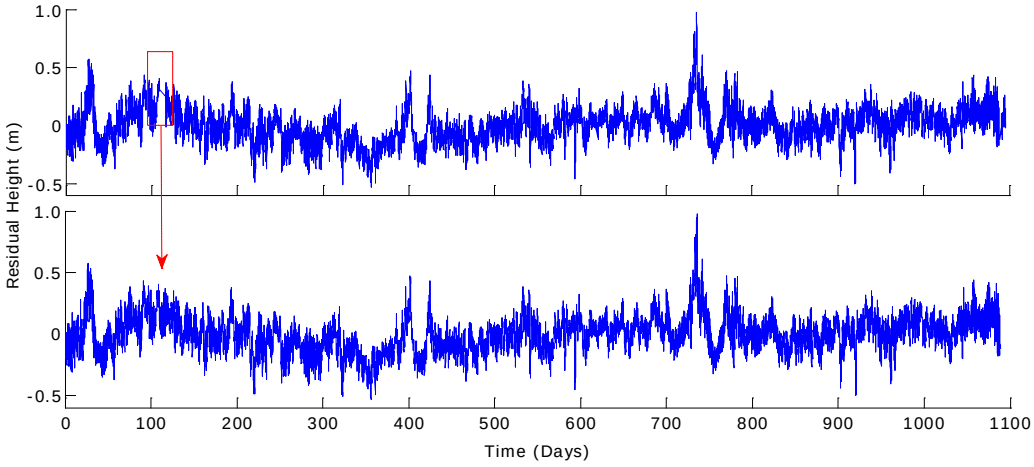


Figure 4.5: a) (top) Booby Island residual time series from January 1, 2006 – December 31, 2008 (AMSA) with data gab, b) (bottom) residual time series with simulated gab.

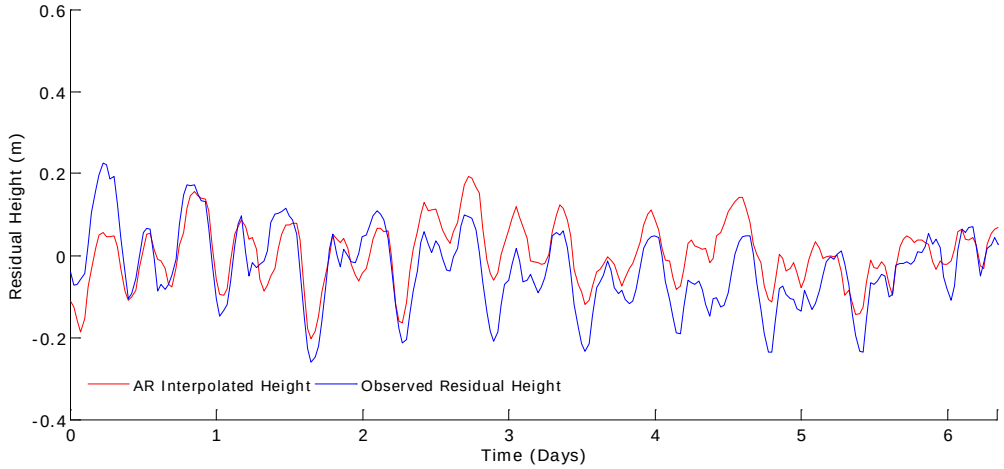


Figure 4.6: Simulated 6 day gab spanning from 19/04 – 06/07/2007, versus residual height (AMSA).

## 4.3 Harmonic Analysis

.

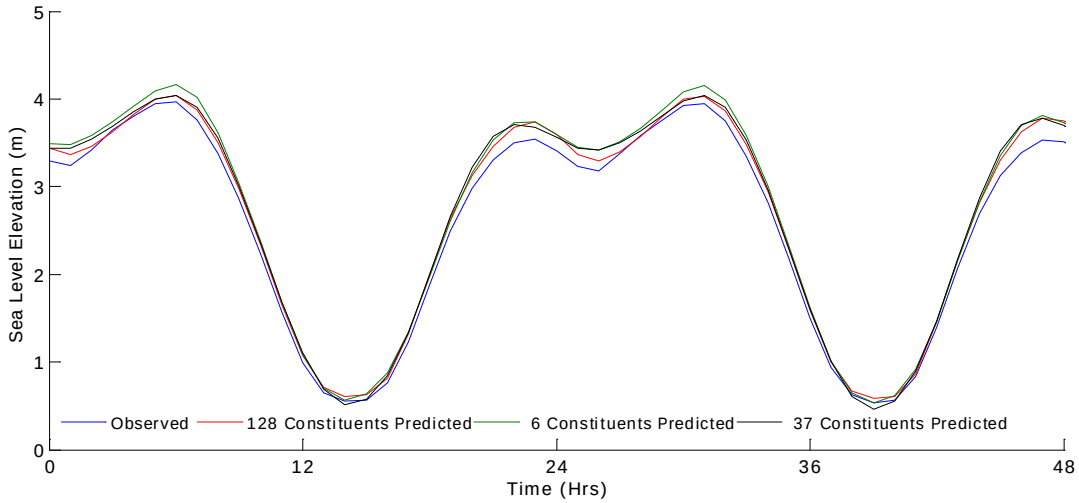


Figure 4.7: Comparison of prediction accuracy of 37, 69, 128 constituent models at Booby Island

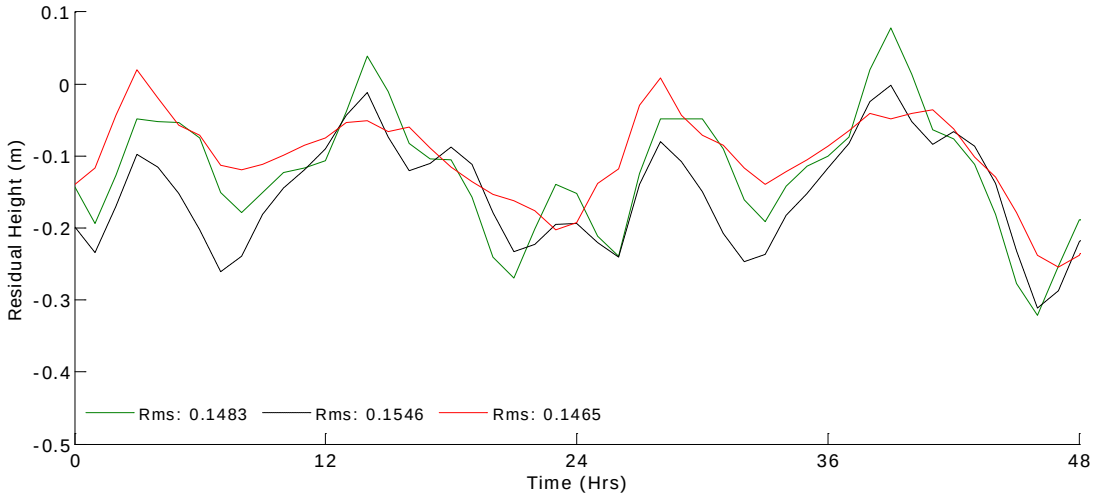


Figure 4.8: Comparison of residual RMS values of 37, 69, 128 constituent models at Booby Island.

| Number of Constituents | Rms (cm) |
|---|---|
| 37 (No shallow water constituents) | 15.46 |
| 69 (Standard package Godin 1973) | 14.83 |
| 128 (Major + Shallow water, Hanxing 1984) | 14.65 |
| 112 (National Tidal Centre) | 14.73 |

Table 4.1: Comparison of Rms values using different constituent models

| Comparison of prediction accuracy of models | | | | |
|---|---|---|---|---|
| Areas | Torres Strait, Australia | | | |
| Stations | Booby Island | | | |
| Constituents | 37 | 128 | 69 | 128 |
| Std σ (Residual, cm) | 15.46 | 14.65 | 14.83 | 14.65 |
| a)% (σ37 –σ128)/(σ128) | 6 | | 1 | |
| b)% (σ69 –σ128)/(σ128) | | | | |

Table 4.2: Accuracy of tidal models

A combination of 128 constituents has shown to be most accurate in the prediction analysis. The standard package by Godin shows a minimal higher standard deviation while using about half the constituents. Even though Godin's standard package performs with sufficient accuracy, the 128 constituent package will be used due to inclusion of more shallow water constituents. The constituent selection is primarily based on the Rayleigh Criterion (Godin 1972). In addition, it has been taken into consideration that shallow water constituents may be diurnal or semi-diurnal in origin.

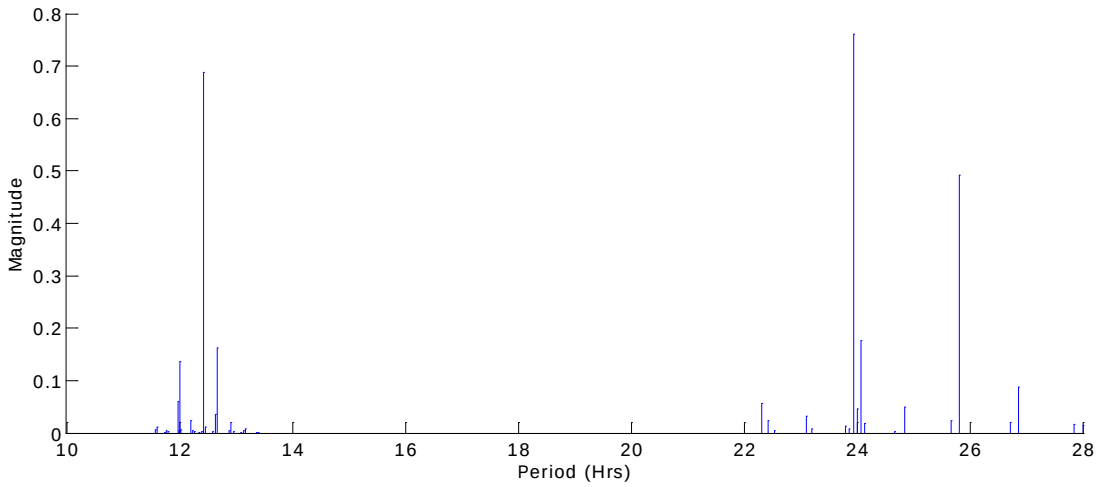


Figure 4.9: Power spectral density of sea level at Booby Island. Dominating tidal energies found analyzing tidal data from 2006-2008 using 128 constituents. 90% of tidal energy is found within this range of frequencies ($M_2$, $N_2$, $S_2$, $K_1$, $O_1$, $K_2$, $Q_1$, Appendix A)

The most dominant tidal amplitudes found at Booby Island Station are the principal lunar (M2) and principal solar ($S_2$). Diurnal constituents such as the principal lunar diurnal ($O_1$) and the luni-solar diurnal also dominate the amplitudes (Appendix 1).

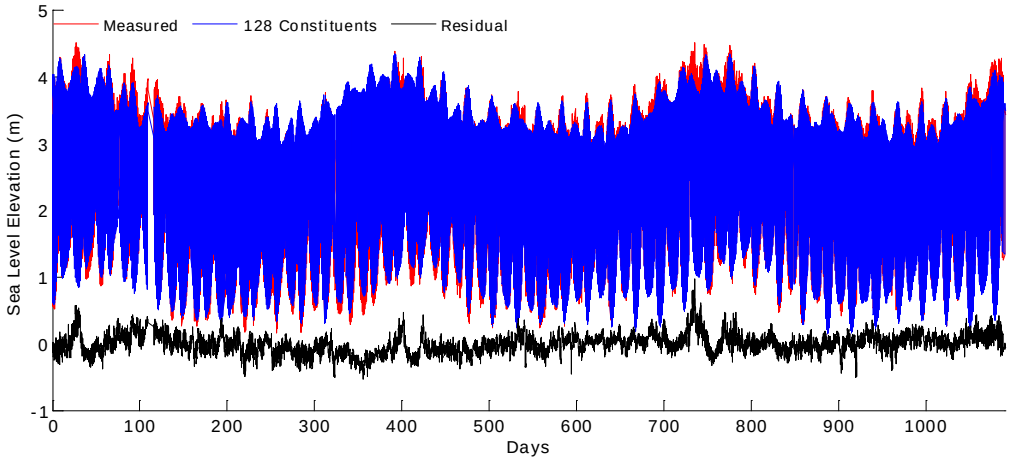


Figure 4.10: Comparison between observed and predicted sea level at Booby Island tide gauge using the 128 shallow water constituent package (Xu). Time is given as from January 1, 2006-2008.

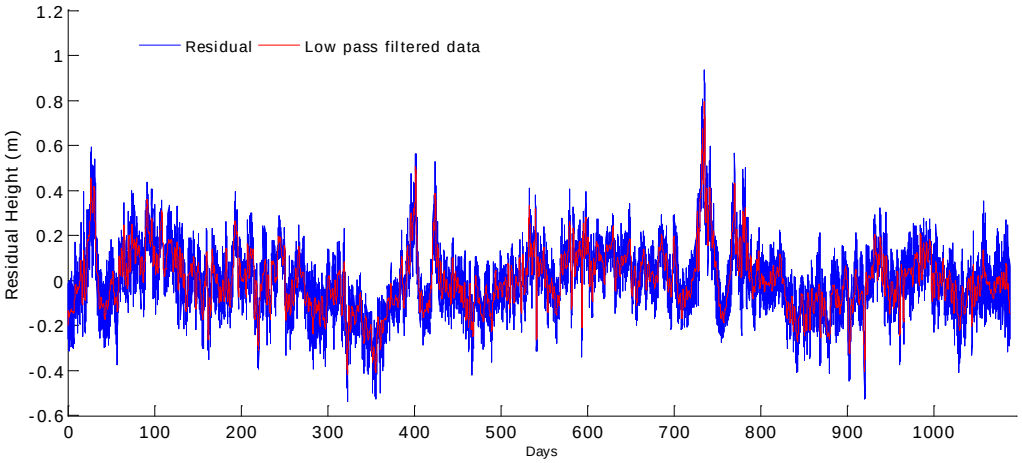


Figure 4.11: Reconstructed residual tidal signal at Booby Island with low pass filtered data at a cut off period of 24 hours.

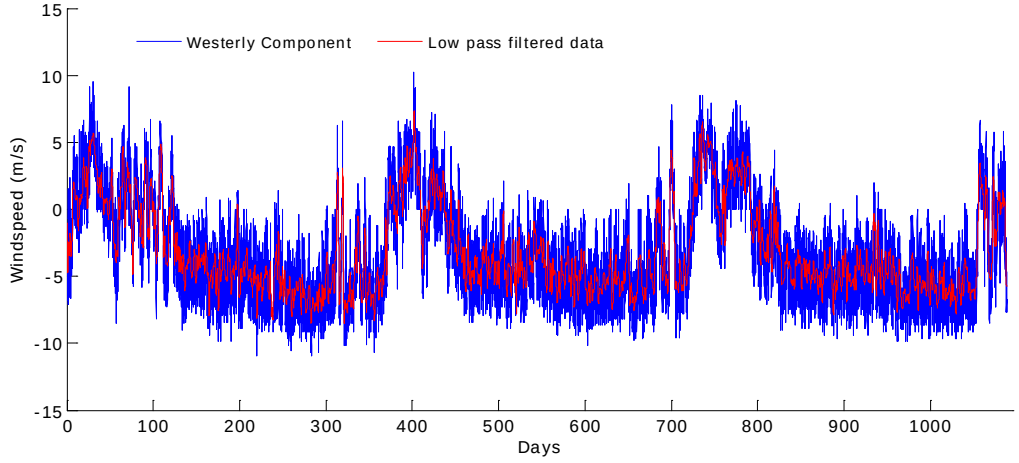


Figure 4.12: Westerly component and low pass filtered data at a cut off period of 24 hours.

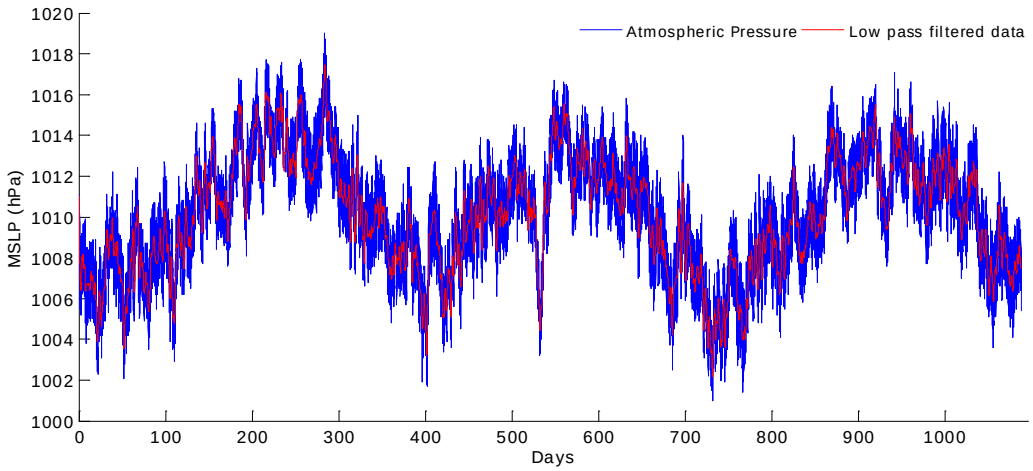


Figure 4.13: Atmospheric pressure and low pass filtered data at a cut off period of 24 hours.

| Correlation coefficients | | |
|---|---|---|
| Station | West Wind (AMSA) | Atmospheric Pressure (AMSA) |
| Booby Island | 0.4499 | -0.4077 |
| Goods Island | 0.3966 | -0.3712 |
| Turtle Head | 0.2094 | -0.3188 |
| Nardana Patches | 0.0841 | -0.0340 |
| Ince Point | 0.0467 | -0.2399 |

Table 4.3: Cross - Correlation coefficients for main tide gauge stations and meteorological parameters obtained using tidal residuals by AMSA. 0 indicates no linear relationship, 1: linear relationship, -1: anti-correlation. Booby Island data shows the strongest response to westerly winds.

| Correlation Coefficients , Low Pass Filtered | | |
|---|---|---|
| Station | | |
| Booby Island | HA(128) | AMSA |
| West Wind (m/s) | 0.4599 | 0.5522 |
| Wind stress | 0.4585 | 0.5650 |
| Atmospheric Pressure (hPa) | -0.3050 | -0.4784 |

Table 4.4: Cross-Correlation coefficients for low pass filtered residual tidal signal and meteorological data. Low frequency time series were obtained by applying a low pass filter to Booby Island reconstructed residual times series (HA 128 ), residual time series (AMSA) and meteorological data (BOM).

## 4.4 Regression Analysis

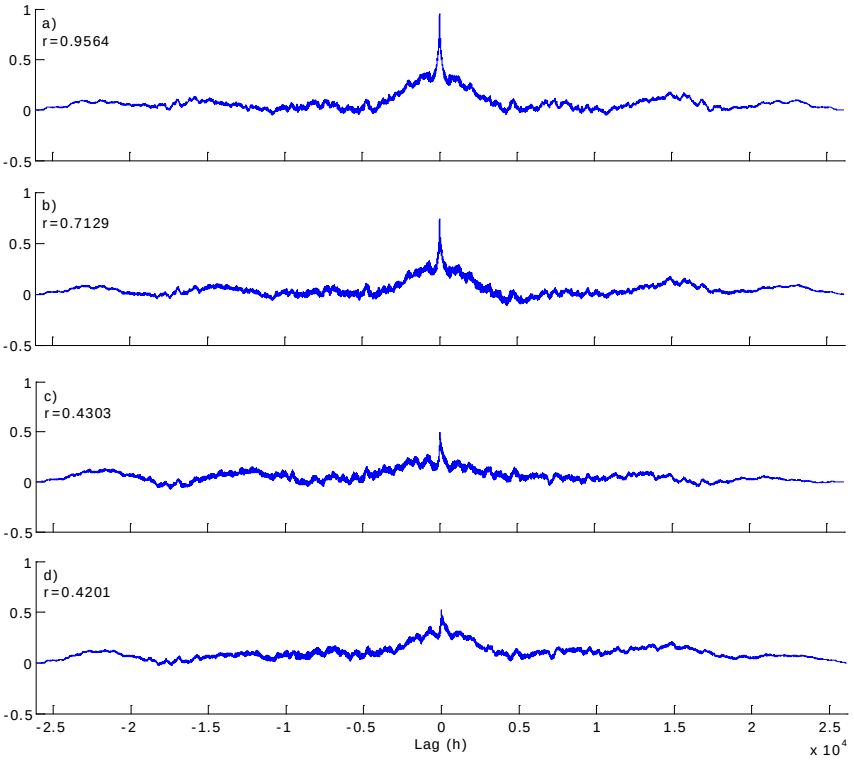


Figure 4.14: Cross correlation functions of Booby Island residuals with tidal residuals from (a) Goods Island, (b) Turtle Head, (c) Nardana Patches and (d) Ince Point. r represents the correlation coefficient.

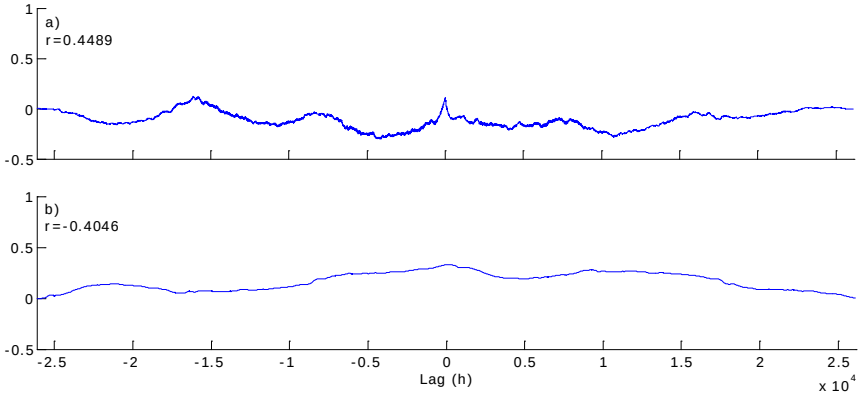


Figure 4.15: Cross correlation functions of Booby Island residuals (a) with u-component of wind at Horn Island, (b) with atmospheric pressure. r represents the correlation coefficient

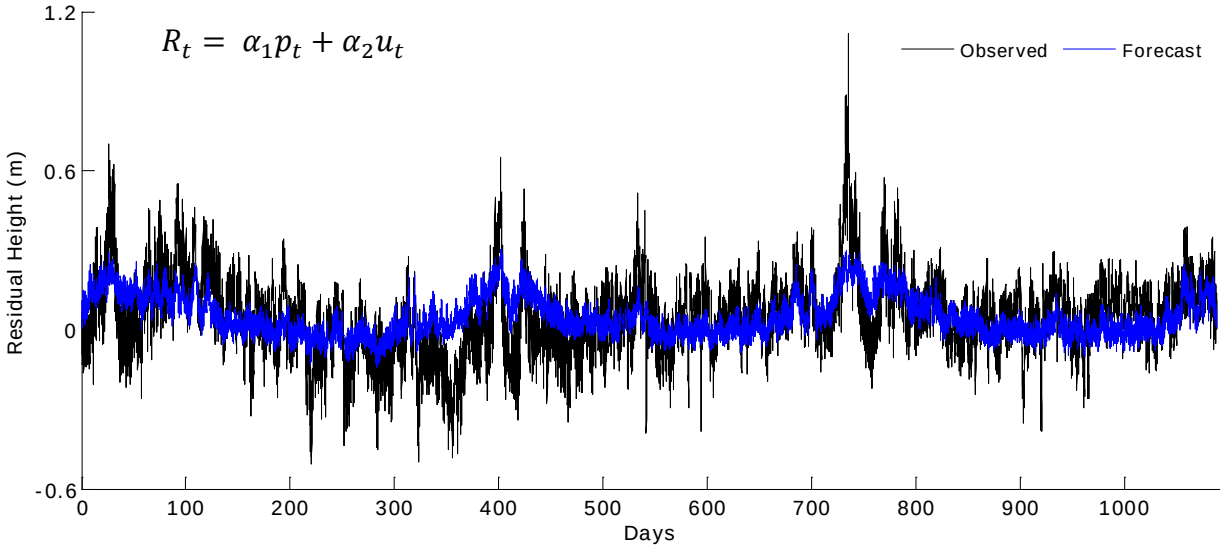


Figure 4.16: Predicted residual sea level at Booby Island. Correlation is 0.4907 with $\boldsymbol{\alpha_1 = -0.2329, \alpha_2 = 0.3263}$

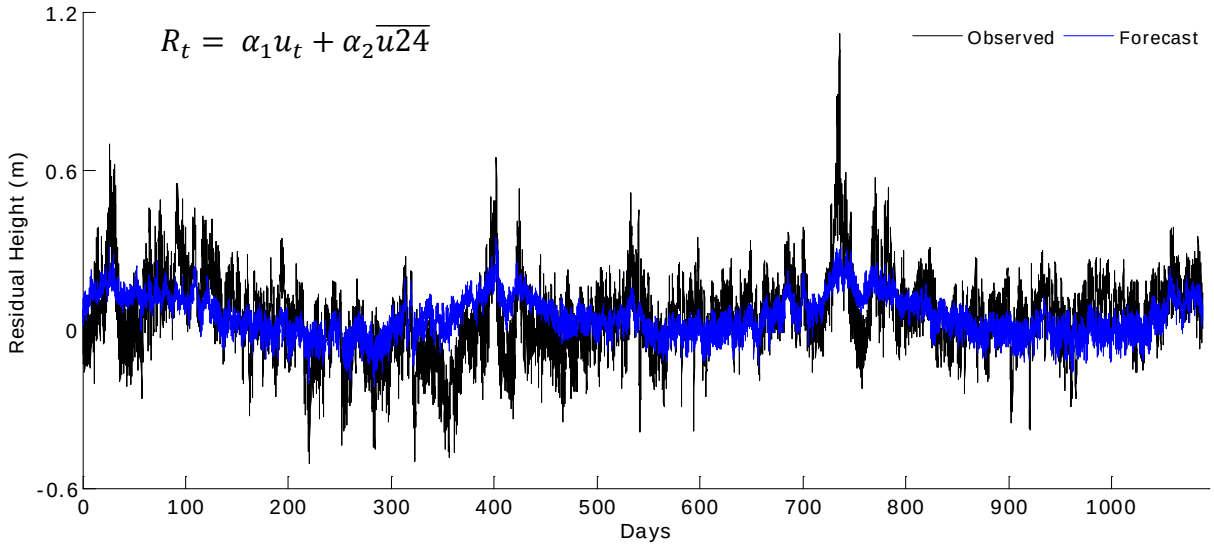


Figure 4.17: Predicted residual sea level height at Booby Island. Correlation is 0.4839 with $\alpha_1 = -0.2563, \alpha_2 = 0.3041$

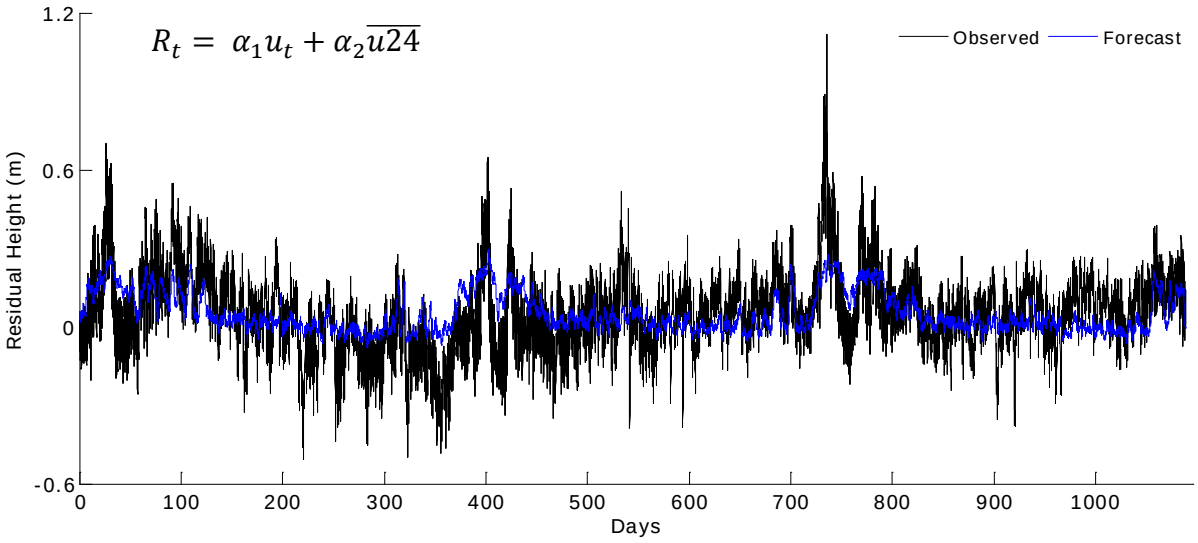


Figure 4.18: Predicted residual sea level height at Booby Island. Correlation is 0.4923 with $\alpha_1 = 0.1072, \alpha_2 = 0.3970$ *where* $\overline{u24}$ is the average of the previous 24 hour wind speed (west component only).

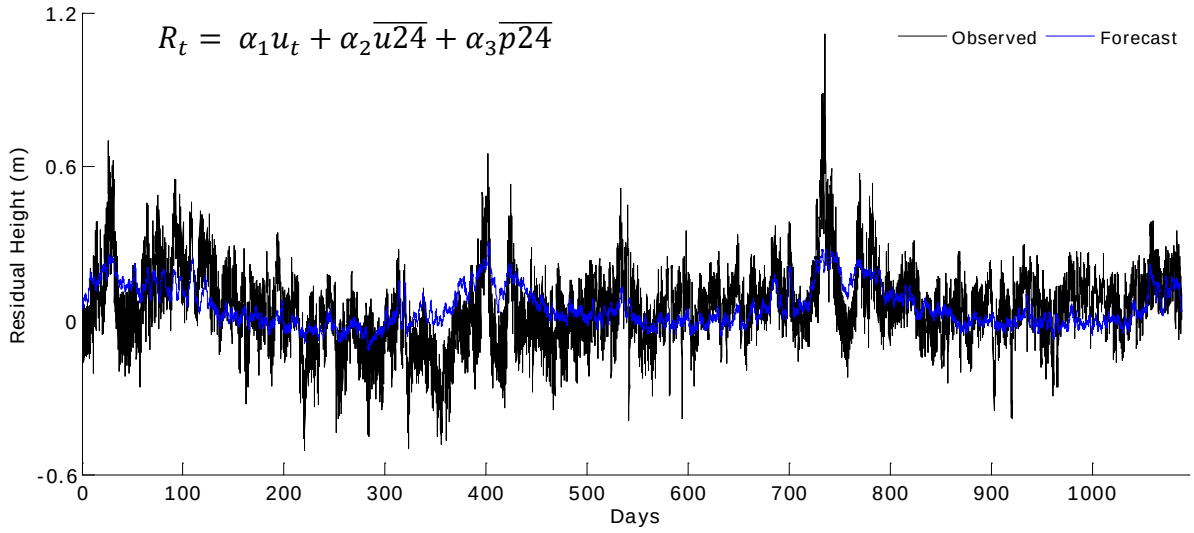


Figure 4.19: Predicted residual sea level height at Booby Island. Correlation is 0.5182 with $\alpha_1 = 0.0934, \alpha_2 = 0.2651, \alpha_3 = -0.2164,$ *where* $\overline{u24}$ is the average of the previous 24 hour wind speed (west component only) and $\overline{p24}$ is the average of the previous 24 hours of atmospheric pressure.

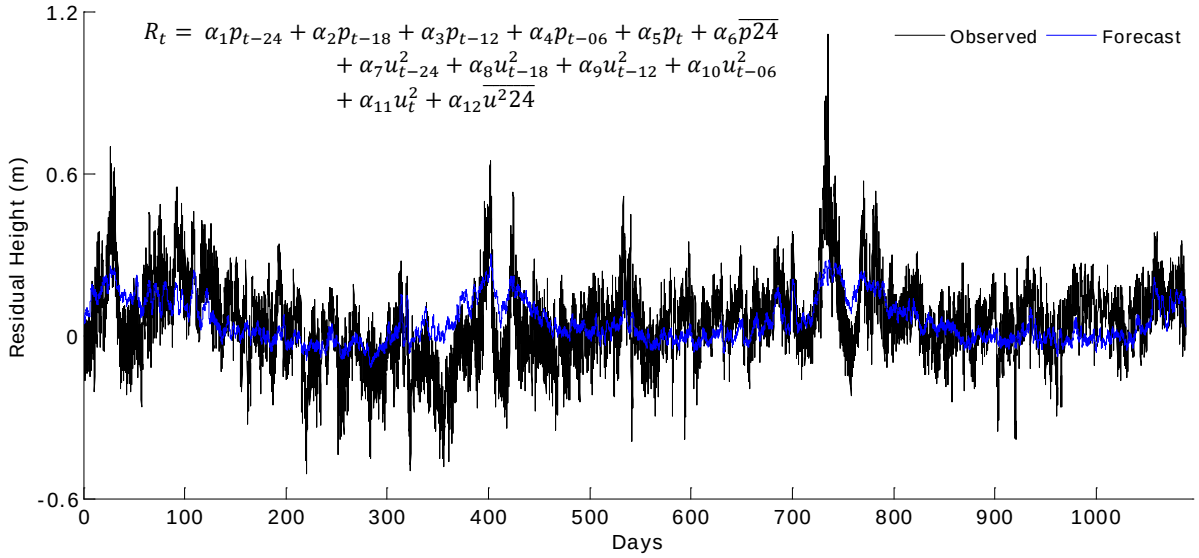


Figure 4.20: Predicted residual sea level height at Booby Island. Correlation is 0.5285 with $\alpha_1 = -0.1331, \alpha_2 = 0.0038, \alpha_3 = 0.0856, \alpha_4 = -0.0035, \alpha_5 = 0.0765, \alpha_6 = -0.2285, \alpha_7 = -0.1168, \alpha_8 = -0.0156, \alpha_9 = -0.0014, , \alpha_{10} = 0.04928, \alpha_{11}\ 0.1356, \alpha_{12} = 0.3211$ *where* $\overline{u^2 24}$ is the average of the previous 24 hour wind stress (west component only) and $\overline{p24}$ is the average of the previous 24 hours of atmospheric pressure.

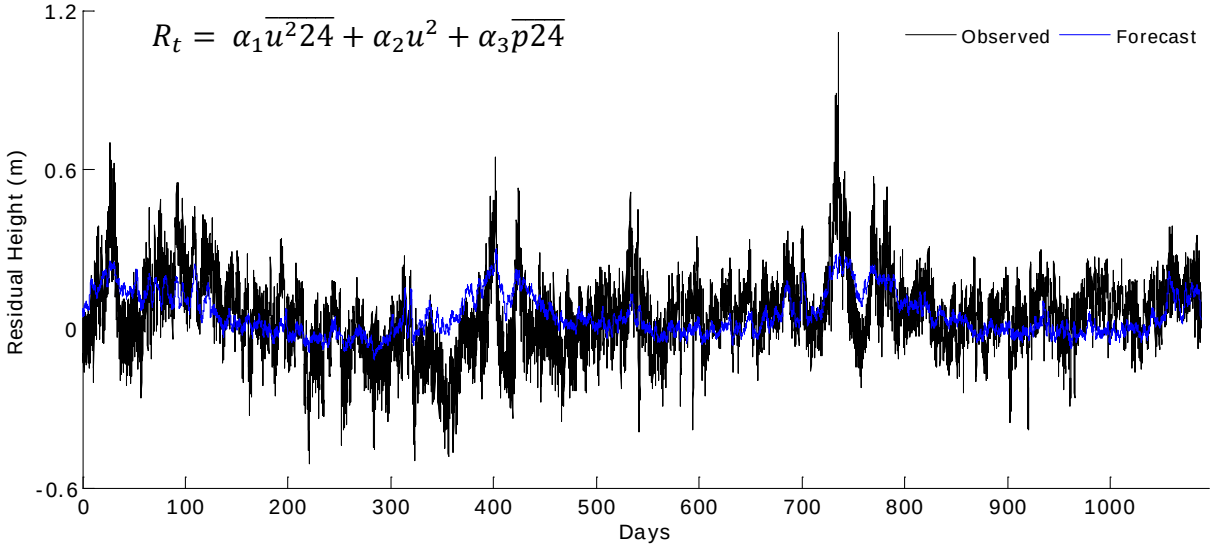


Figure 4.21: Predicted residual sea level height at Booby Island. Correlation is 0.5218 with $\alpha_1 = 0.3020, \alpha_2 = 0.0741, \alpha_3 = -0.2014$

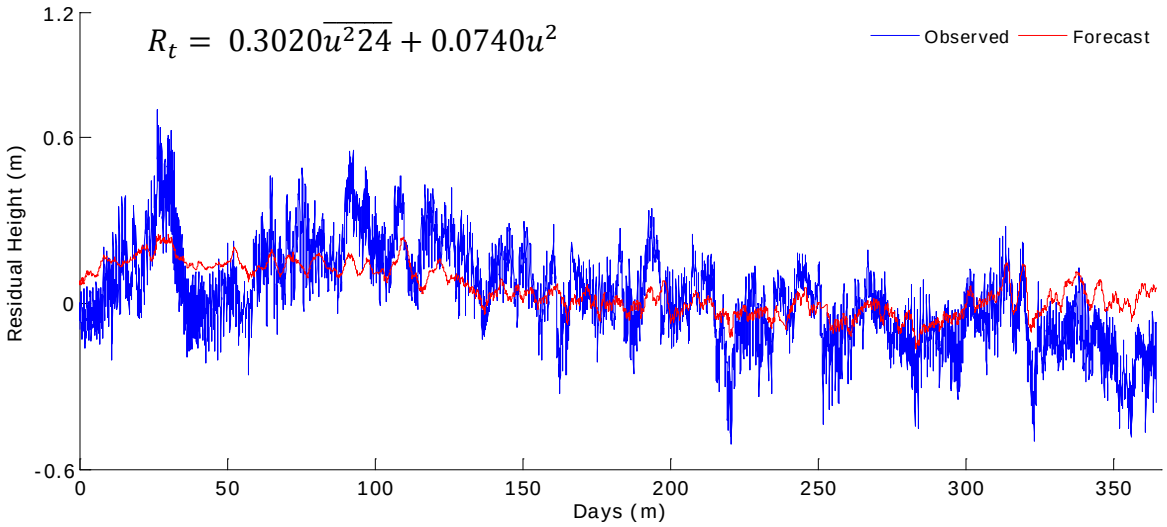


Figure 4.22: Final residual height forecast (Booby Island) for 360 days in 2006. Residual heights computed from observed /predicted sea level heights by AMSA, and meteorological residual forecast obtained using meteorological data. Linear correlation between forecast and residual data is 0.6294.

# Chapter 5. Discussion and Conclusions

In the introduction to the thesis, it was hypothesized that non-periodical tidal residuals were mainly the result of meteorological forcing mechanisms such as west wind and atmospheric pressure. This hypothesis was not fully confirmed by the findings of this study. The approach presented here is similar to that used in Amin (1978), but it differs in its approximation of time lags and input parameters. A positive correlation for westerly winds was established by applying cross correlation functions of tidal residuals of Booby Island, Turtle Head, Nardana Patches and Ince Point with meteorological parameters (Figure 4.15 and 4.15, Table 4.3 and 4.4). However, with increasing distance from Booby Island the correlation decreases in magnitude resulting in no significant correlation at Turtle Head, Nardana Patches and Ince Point.

The response of residual sea level to barometric pressure is found to be most significant during periods of low pressure systems (Figure 4.4). Weather maps for the surrounding Torres Strait region are fairly complex, with fast changing patterns. This fact makes is extremely difficult to conclude spatial variations since only one weather station placed at Horn Island airport has been used. The coefficient associated with the westerly component of wind, suggests that Booby Island, located at the western end of the Prince of Wales Channel, is most effected by west winds and thus more likely to develop higher residuals. The cross correlation functions of Booby residuals with residuals from the other 4 ports (Figure 4.14), confirm Wolanski's findings in 1988 that the western and eastern part of the Prince of Wales Channel are incoherent. This could result in a buildup in the event of strong westerly winds due to reversed tidal flow entering from the Coral Sea (Wolanski 1988).

Tropical cyclones originating in the Gulf of Papua and the Coral Sea are considered with the occurrence of extreme water level fluctuations in the Torres Strait region. This conforms with Amin's (1978) findings regarding the effects of synoptic scale meteorological events on residual water level fluctuations in this region. The

statistical analysis of tropical cyclones shows that one storm every two years hits the Gulf of Papua and western Torres Strait region, with a higher frequency of occurrence in the Coral Sea. This could result not only in extreme storm surges, but also in interannual oscillation anomalies.

The equations shown in Figure 4.16 to 4.22, show that time lags of 24 hours prove to be most successful. Depending on the wind speed, direction and duration, sea level response may vary. Therefore, the most significant time lag has been shown to be an average of the previous 24 hours of data. As a result, a combination of a 24 hour time lag along with the average of the previous 24 hours and the current data with no time lag, offers the best solution to the system (17). This equation (19) allows for the inclusion of weather systems impacting the area within the last 24 hours as well as it takes into account the current conditions. The main focus of this project was to develop a system using real time residual sea level data, given by AMSA, and real time meteorological data to forecast and investigate errors in tidal predictions. Hence, tidal data by AMSA was used for testing the model, whereas reconstructed residual sea levels were used for spectral analysis.

It is observed that the linear forecasting regime tends to under predict the amplitude of the residuals and discrepancies are visible between the observed and forecast residual tidal signal. Therefore, the corresponding water level fluctuation cannot be well predicted. As to the water level variations due to westerly winds, prediction is based on the correlation between the residual water level at the time and the tendency of the previous correlation with meteorological input parameters. However, there appears to be no simple method for forecasting tidal residuals using meteorological data in Torres Strait. The regression technique, as described in equation (19), is a linear process and does not adequately include non-linear effects contributing to the residual sea level. The difficulty of the procedure is associated with the complexity of the tidal regimes governing this area. The forecasting scheme did prove not to be successful, but that does not lead to the conclusion that no interaction between meteorology and residuals exists. It is assumed that this simple model cannot simulate the complex tidal regime in Torres Strait.

In a future study, a more careful analysis of the data with regards to low and high frequency residual sea level fluctuations is suggested to investigate topographical induced seiches. Further theoretical work on the Arafura Sea-Gulf system is needed to gain a better understanding of oscillations in central Torres Strait.

# Acknowledgements

I would like to thank my advisor Dr. Tim Gourlay (CMST) and co advisor Dr. Kim Klaka (CMST) for the invaluable assistance and patience they gave me. A great thank you also goes to Dr. Alec Duncan (CMST) and Dr. Brendan Mcgann. The thesis is also dedicated to the Australian Reef Pilots in Torres Strait, who successfully maneuver through this difficult stretch of water for years and counting.

# Appendices

## A1. Harmonic Analysis

## A2. Spectral Analysis

## A1. Harmonic Analysis

| Symbol | Name | Period (hours) |
|---|---|---|
| $M_2$ | Principal lunar | 12.42 |
| $N_2$ | Larger lunar elliptic | 12.66 |
| $S_2$ | Principal solar | 12 |
| $K_1$ | Luni-solar diurnal | 23.93 |
| $O_1$ | Principal lunar diurnal | 25.82 |
| $K_2$ | Luni-solar semi-diurnal | 11.97 |
| $Q_1$ | Larger lunar elliptic | 26.87 |

Table A1: Dominating Tidal Constituents found in the tidal signal at Booby Island (2006 – 2008)

| List of 128 constituents | | | | | |
|---|---|---|---|---|---|
| Constituents | | Period (h) | Constituents | | Period(h) |
| No. | Name | | No. | Name | |
| 1 | Sa | 8765.821090 | 65 | 3MS4 | 6.321078 |
| 2 | Ssa | 4382.905209 | 66 | MN4 | 6.269174 |
| 3 | Sa3 | 2921.937992 | 67 | MNKS4 | 6.260219 |
| 4 | Sa4 | 2191.452604 | 68 | M4 | 6.210301 |
| 5 | MSm | 778.820580 | 69 | SN4 | 6.160193 |
| 6 | Mm | 661.309205 | 70 | KN4 | 6.048197 |
| 7 | SMm | 614.918644 | 71 | MS4 | 6.106445 |
| 8 | MSf | 354.367052 | 72 | MK4 | 6.094852 |
| 9 | Mf | 327.858969 | 73 | SL4 | 6.047526 |
| 10 | SaMf | 316.038506 | 74 | S4 | 6.000000 |
| 11 | Mtm | 219.190386 | 75 | SK4 | 5.991797 |
| 12 | 2Q1 | 28.006223 | 76 | MNO5 | 5.044357 |
| 13 | sig1 | 27.848388 | 77 | 2MO5 | 5.006171 |
| 14 | Q1 | 26.868357 | 78 | 3MP5 | 5.000460 |
| 15 | rho1 | 26.723053 | 79 | MNK5 | 4.967922 |
| 16 | O1 | 25.819342 | 80 | 2MP5 | 4.936434 |
| 17 | MP1 | 25.668133 | 81 | 2MK5 | 4.930880 |
| 18 | M1 | 24.841202 | 82 | MSK5 | 4.863211 |
| 19 | x1 | 24.663366 | 83 | 3KM5 | 4.857820 |
| 20 | pi1 | 24.132140 | 84 | 3NKS6 | 4.215391 |
| 21 | P1 | 24.065890 | 85 | 2NM6 | 4.192698 |
| 22 | S1 | 24.000000 | 86 | 2NMKS6 | 4.188691 |
| 23 | K1 | 23.934470 | 87 | 2MN6 | 4.166284 |
| 24 | psi1 | 23.869299 | 88 | 2MNKS6 | 4.162327 |
| 25 | phi1 | 23.804477 | 89 | M6 | 4.140200 |
| 26 | theta1 | 23.206957 | 90 | MSN6 | 4.117870 |
| 27 | J1 | 23.098477 | 91 | MKN6 | 4.114005 |
| 28 | 2PO1 | 22.535455 | 92 | 2MS6 | 4.092388 |
| 29 | So1 | 22.420178 | 93 | 2MK6 | 4.088570 |
| 30 | OO1 | 22.306074 | 94 | NSK6 | 4.066792 |
| 31 | 2NS2 | 13.393127 | 95 | 2SM6 | 4.045666 |
| 32 | 2NK2S2 | 13.352325 | 96 | MSK6 | 4.041935 |
| 33 | OQ2 | 13.166703 | 97 | S6 | 4.000000 |
| 34 | MNS2 | 13.127267 | 98 | 2MNO7 | 3.587409 |
| 35 | MNK2S2 | 13.088067 | 99 | 2NMK7 | 3.567725 |
| 36 | 2MS2K2 | 12.947808 | 100 | 2MSO7 | 3.532486 |
| 37 | 2N2 | 12.905374 | 101 | MSKO7 | 3.494831 |
| 38 | mu2 | 12.871758 | 102 | 2(MN)8 | 3.134587 |
| 39 | N2 | 12.658348 | 103 | 3MN8 | 3.119799 |
| 40 | v2 | 12.626004 | 104 | 3MNKS8 | 3.117580 |
| 41 | 2KN2S2 | 12.585651 | 105 | M8 | 3.105150 |
| 42 | OP2 | 12.455900 | 106 | 2MSN8 | 3.092573 |
| 43 | M2 | 12.420601 | 107 | 2MNK8 | 3.090392 |
| 44 | MKS2 | 12.385502 | 108 | 3MS8 | 3.078178 |
| 45 | M2(KS)2 | 12.350601 | 109 | 3MK8 | 3.076017 |
| 46 | 2SN(MN)2 | 12.255950 | 110 | MSNK8 | 3.063674 |
| 47 | lam2 | 12.221774 | 111 | 2(MS)8 | 3.051670 |
| 48 | L2 | 12.191620 | 112 | 2MSK8 | 3.049546 |
| 49 | T2 | 12.016449 | 113 | 2M2NK9 | 2.771603 |
| 50 | S2 | 12.000000 | 114 | 3MNK9 | 2.760035 |
| 51 | R2 | 11.983596 | 115 | 4MK9 | 2.748564 |
| 52 | K2 | 11.967235 | 116 | 3MSK9 | 2.727409 |
| 53 | MSN2 | 11.786131 | 117 | 4MN10 | 2.493487 |
| 54 | Kj2 | 11.754522 | 118 | M10 | 2.484120 |
| 55 | 2KM(SN)2 | 11.723082 | 119 | 3MNS10 | 2.476064 |
| 56 | 2SM2 | 11.606952 | 120 | 4MS10 | 2.466828 |
| 57 | SKM2 | 11.576295 | 121 | 2MNSK10 | 2.457504 |
| 58 | NO3 | 8.494019 | 122 | 3M2S10 | 2.449774 |
| 59 | 2MK3 | 8.386303 | 123 | 4MSK11 | 2.236338 |
| 60 | M3 | 8.280401 | 124 | M12 | 2.070100 |
| 61 | SO3 | 8.192424 | 125 | 4MNS12 | 2.064503 |
| 62 | MK3 | 8.177140 | 126 | 5MS12 | 2.058078 |
| 63 | SK3 | 7.992706 | 127 | 3MNKS12 | 2.051584 |
| 64 | N4 | 6.329174 | 128 | 4M2S12 | 2.046194 |

Table A2 : 128 constituents which have been previously chosen for a 1 year long time series in the shallow ports of Shanghai by Xu in 1984.

## A2.Spectral Analysis

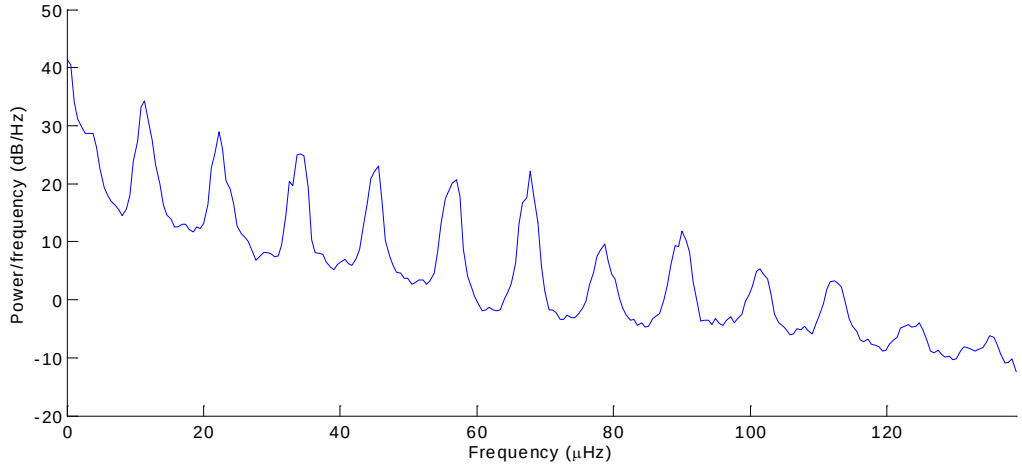


Figure A1: Welch Power Estimate. Reconstructed residual sea level height

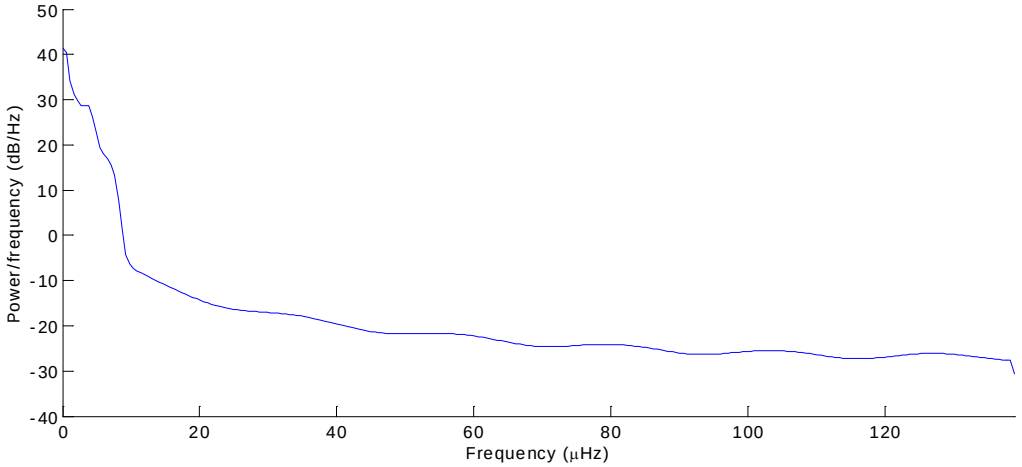


Figure A2: Welch Power Estimate. After Butterworth low pass filter applied to residual data.

# References


Amin, M. 1978. A statistical analysis of storm surges in Torres Strait. *Australian Journal of Marine Freshwater Research* 29: 479-496.

Andrews, J.C., Clegg, S., 1989. Coral Sea circulation and transport from model information models. *Deep Sea Research* 36: 957-974.

Andrews, J.C., Furnas, M.J., 1986. Subsurface intrusions of Coral Sea water into the central Great Barrier Reef. *Continental Shelf Research* 6: 491-514.

Bode, L., Mason, L., 1994. Tidal modeling in Torres Strait and the Gulf of Papua. *Recent Advances in Marine Science and Technology '94. James Cook University of North Queensland, Townsville.*

Bowden, F., Hamilton, P., 1975. Some experiments with a numerical model of circulation and mixing in a tidal estuary. *Estuarine and Coastal Marine Science* 3: 281-301.

Church, J.A., Boland, F.M., 1983. A permanent under current adjacent to the Great Barrier Reef. *Journal of Physical Oceanography* 13: 1747 - 1749.

Clarke, A.J., 1990. Application of a frictional channel flow theory to flow in the Prince of Wales Channel, Torres Strait,' *Journal of Physical Oceanography* 20 (6) 890 - 899.

Condie, S., Margvelashvili, Saint-Cast, F. 2008. Numerical modeling of the suspended sediment transport in Torres Strait. *Continental Shelf Research* 28: 2241 - 2258.

Csanady,G.T. 1973.Wind-driven barotropic motions in long lakes. *Journal of Physical Oceanography* 3: 429 - 438.

Daniell, J., Hughes, M. 2007. The morphology of barchans-shaped sand banks from western Torres Strait, northern Australia. *Sedimentary Geology* 202: 638 - 652.

Deleersnijder, E., Norro, A., Wolanski, E., 1992. A three dimensional model of the water circulation around an island in shallow waters. *Continental Shelf Research* 12: 89 - 906.

Donguy, J. R., Henin, C. 1975. Surface waters in the north of the Coral Sea. *Australian Journal of Marine and Freshwater Research* 26: 293-296.

Dyer, K.R., Huntley, D.A., 1999. The origin, classification and modeling of sand banks and ridges. *Continental Shelf Research* 19: 1285 - 1330.

Forbes, A., Church, J. 1983. Circulation of the Gulf of Carpentaria. Residual currents and mean sea level. *Australian Journal of Marine Freshwater Research* 34: 11 - 22.

Foreman, M. 1977. Manual for tidal height analysis and prediction. *Pacific Marine Science* 77: 97. Institute of Ocean Sciences, Patricia bay, British Columbia.

Foreman, M., Neufeld, E.T., 1991. Harmonic tidal analyses of long time series. *International Hydrographic Review* 68 (1): 85 - 108.

Furukawa, K., Wolanski, E., 1998. Shallow water frictional effects in island wakes. *Estuarine, Coastal and Shelf Science* 46: 599-608.

Godin, G., 1972. *The analysis of tides*. University of Toronto Press, Toronto.

Grant, W. D., Madsen, O.S., 1979. Combined wave and current interaction with a rough bottom. *Journal of Physical Oceanography* 84: 1797 - 1808.

Harris, P.T., 1989. Sand wave movement under tidal and wind-driven currents in a shallow marine environment: Adolphus Channel, north-eastern Australia. *Continental Shelf Research* 9 (11): 981 - 1002.

Jay, D.A., Flinchem, E.P., 1999. A comparison of methods for analysis of tidal records containing multi-scale non-tidal background energy. *Continental Shelf Research* 19: 1695 – 173

King,B., Norrot, A., Wolanski, E., 1995. Water circulation in the Gulf of Papua.*Continental Shelf Research* 15 (2/3): 185-212.

Knight, J.H., 1981, Steady periodic flow through a rectangular dam. *Water Resource Research* 17: 1222-1224.

Lemckert, C., Zier, J., Gustafson, J., 2009. Tides in Torres Strait. *Journal of Coastal Research* 56: 524 – 528.

McMurtree, R., Webb, D.J. 1975. Tidal response functions around Australia from harmonic constants. *Australian Journal of Marine Freshwater Research* 26: 245-69.

Middelton, J.H., 1987. Steady coastal circulation due to oceanic longshore pressure gradients. *Journal of Physical Oceanography* 17: 604-612.

Nielson, P., 1990. Tidal dynamics of the water table in beaches. *Water Resource Research* 26: 2127 - 2134.

Okubo, S., 1974. Effects of shoreline irregularities on streamwise dispersion in estuaries and other embayments. *Netherlands Journal of Sea Research* 6: 213 - 224.

Off, T., 1963. Rhythmic linear sand bodies caused by tidal currents. *Bulletin of the American Association of Petroleum Geologists* 47(2): 324 - 341

Pawlowicz, R., Beradsley, B., Lentz, S., 2002. Classical tidal harmonic analysis including error estimates in MATLAB usingT_TIDE. *Computers and Geosciences* 28: 929 - 937.

Provis, D., Lennon,G.W. 1983. Eddy viscosity and tidal cycles in a shallow sea. *Estuarine Coastal Shelf Science* 16: 351 - 361.

Rigeway, K.R., Dunn, J.R., Wilkin, J.L., 2002. Ocean interpolation by four dimensional weighted least squares- applications to the waters around Australiasia. *Journal of Atmospheric and Oceanic Technology* 19: 1357 - 1375.

Robinson, C., Li, L., Barry, D.A., 2007. Effect of tidal forcing on a subterranean estuary. *Advances in Water Resources* 30: 851-865.

Rochford, D., 1966, 'Some hydrological features of the Eastern Arafura Sea and the Gulf of Carpentaria in August 1964,' *Australian Journal of Marine Freshwater Research*, vol. 17, pp. 31 - 60.

Saint-Cast, F. 2008. Multiple time-scale modeling of the circulation in Torres Strait-Australia. *Continental Shelf Research* 28: 2214 - 2240.

Saint-Cast, F., Condie, S., 2006. Circulation modeling in Torres Strait. *Geoscience in Australia,* Record 2006 (18): 82.

Webb, D.J. 1981. Numerical Model of the tides in the Gulf of Carpentaria and Arafura Sea. *Australian Journal of Marine Freshwater Research* 32: 31 - 44.

Wolanski, E., 1983. Tides on the northern Great Barrier Reef continental shelf. *Journal of Geophysical Research* 88: 5953 - 5959.

Wolanski, E. 1993. Water circulation in the Gulf of Carpentaria. *Journal of Marine System* 4: 401 - 420.

Wolanski, E., Drew, E., Abel, K., O'Brien, J., 1988. Tidal jets, nutrient upwelling and their influence on the productivity of the algal Halimeda in the Ribbon Reefs, Great Barrier Reef. *Estuarine, Coastal and Shelf Science* 26: 169 - 201.

Wolanski, E., 1994. Physical oceanographic processes of the Great Barrier Reef. *CRC Press, Australia.*

Wolanski, E., King, B., 1990. Flushing of Bowden Reef lagoon, Great Barrier Reef. *Estuarine. Coastal and Shelf Science* 31: 789 - 804.

Wolanski, E., Pickard,G., Jupv,D. 1984. River plumes, coral reefs and mixing in the Gulf of Papua and the northern Great Barrier Reef,' *Estuarine, Coastal and Shelf Science* 18: 291-314.

Wolanski, E., Ridd, P., Inoue, M. 1988. Currents through Torres Strait. *Journal of Physical Oceanography* 18: 1535 - 1545.

Wolanski, E., Ruddick,B., 1981. Water circulation and shelf waves in the northern Great Barrier Reef lagoon. *Australian Journal of Marine and Freshwater Research* 32: 721 - 740.

Wolanski, E., Spagnol, S., 2000. Sticky waters in the Great barrier reef. *Estuarine, Coastal and Shelf Science* 50: 27 - 32.

Wolanski, E., Thompson, R. 1984. Wind-driven circulation on the northern Great Barrier Reef continental shelf in summer. *Estuarine, Coastal and Shelf Science* 18: 271 - 289.

Wyrtki, K., 1962. Geopotential topographies and associated circulation in the western South Pacific ocean. *Australian Journal of Marine and Freshwater Research* 13: 89 - 105.

Van der Molen,J., 2002. The influence of tides, wind and waves on the net sand transport in the North Sea. *Continental Shelf Research* 22: 2739 – 2762